# Red Hot Fluorine $^{19}$F MRI & SAMS meet Kraków MRI Workshop 2023

## December 4-6, 2023
## Kraków, Poland

Organized by:

**H. Niewodniczański Institute of Nuclear Physics**
**Polish Academy of Sciences**

Venue: Institute of Nuclear Physics PAN,
Main Building, Auditorium
Radzikowskiego 152, Kraków, Poland

Partners:

**Agenda**

**Monday, December 4** IFJ PAN, Main Building, Auditorium

| **Registration** | |
|---|---|
| 10:30 - 11:00 | Registration start & Welcome coffee<br>IFJ PAN, Main Entrance (Radzikowskiego street), 1st Floor |

| **Welcome** | |
|---|---|
| 11:30 - 11:45 | Opening<br>**Prof. dr hab. Tadeusz Lesiak**, Director IFJ PAN, Poland |

| **1. Let's start! Chair: tba** | |
|---|---|
| 11:45 - 12:15 | **Jeff Bulte**, Baltimore, USA<br>Real-Time In Vivo Cytometry using MPI |
| 12:15 - 12:45 | **Cornelius Faber**, Münster, Germany<br>Detecting inflammatory cell migration by MRI |
| 12:45 - 13:15 | **Greg Stanisz**, Toronto, Canada<br>Metabolic MRI: is it useful or confusing? |

| 13:15 - 14:30 | Lunch, IFJ cantine |
|---|---|

| **2. Let's take a look at organisms; Chair: tba** | |
|---|---|
| 14:30 - 15:00 | **Susann Boretius**,Gottingen, Germany<br>MRI in the common Marmoset - Bridge on the way from mouse to human. |
| 15:00 - 15:30 | **Verena Hoerr**, Bonn, Germany<br>Cardiac CEST MRI to identify myocardial infarction |
| 15:30 - 16:00 | **Harald Moeller**,Leipzig, Germany<br>Information on brain tissue microstructure obtained from MRI signal phase |
| 16:00 – 16:30 | **Piotr Kozlowski**, Vancouver, Canada<br>Modelling inhomogeneous magnetization transfer in myelin and intra/extra-cellular water in normal and injured rat spinal cords ex vivo |

| 16:30 - 17:00 | Coffee Break, IFJ cantine |
|---|---|

| **3. $^{1}$H and other nuclei; Chair:tba** | |
|---|---|
| 17:00 - 17:30 | **Daniel Jirak**, Prague, Czech Republic<br>Functional X-nuclei Magnetic Resonance (Reactive Oxygen Species Detection) |
| 17:30 - 18:00 | **Peter Vermathen**, Bern, Switzerland<br>In vivo Potassium MR-Spectroscopy at 7 T. Establishment and first Applications in Human Muscle |
| 18:00 - 18: 20 | **Łukasz Boguszewicz**, Gliwice, Poland<br>$^{1}$H NMR-based metabolomics in head and neck cancer treatment - whether it may be helpful for a clinical? |

| | |
|---|---|
| 18:20 - 18:40 | **Igor Zhukov**, Warsaw, Poland<br>The application of $^{19}$F NMR spectroscopy in biomolecular studies as a potent technique for structural analysis of the proteins and protein-protein complexes in solution |
| 18:40 - 19:00 | **Radovan Jiřík**, Brno, Czech Republic<br>Perfusion MRI on small animals beyond $K^{trans}$ |

**Tuesday, December 5** IFJ PAN, Main Building, Auditorium

| **Registration** | |
|---|---|
| 8:00- 12:00 | Registration, Auditorium Entrance, 1st Floor |

| **4.Let's focus on $^{19}$F; Chair: tba** | |
|---|---|
| 8:30 - 9:00 | **Francesca Baldelli Bombelli**, Milan, Italy<br>Pivotal role of the protein corona on NP cellular uptake for boosting $^{19}$F- MRI sensitivity |
| 9:00 - 9:30 | **Mitchell Albert**, Thunder Bay, Canada<br>Fluorine-19 Magnetic Resonance Imaging of the Lungs using Octafluorocyclobutane |
| 9:30 - 10:00 | ~~**Philipp Boehm-Sturm**, Berlin, Germany~~ (WITHDROWN)<br>~~A no brainer? $^{19}$F MR neuroimaging of cerebrovascular disease~~ |
| 10:00 - 10:30 | **Anton Windfelder**,Giessen, Germany<br>In vivo monitoring of gut inflammation in the insect larvae of Manduca sexta by $^{19}$F magnetic resonance imaging |

| | |
|---|---|
| 10:30- 11:00 | Coffee Break |

| **5. A bit of chemistry (and more); Chair: tba** | |
|---|---|
| 11:00 - 11:30 | **Ulrich Floegel**, Dusseldorf, Germany<br>Molecular Imaging via $^{19}$F MRI |
| 11:30 - 11:50 | **Robbin de Kruijf**, Wageningen, The Netherlands<br>The development and characterisation of an in vivo $^{19}$F MRI imaging agent |
| 11:50 - 12:10 | ~~**Monica Carril**, Leioa, Spain~~ (WITHDROWN)<br>~~Water Dispersible Small Nanoparticles with Fluorinated Surface and High Relaxation Times for $^{19}$F MR Applications~~ |
| 12:10 - 12:30 | **Tomasz Krawczyk**, Gliwice, Poland<br>Design Principles and Potential Applications of Molecular Hydrazone Switches for pH Imaging in $^{19}$F MRI |
| 12:30 - 12:50 | **Wilfried Reichardt**, Freiburg, Germany<br>Tracking of immune cells using $^{19}$F MR imaging in a murine model of pancreatic cancer under therapy |

| | |
|---|---|
| 13:00 - 14:30 | Lunch, IFJ cantine |

| 6. A bit of imaging technics; Chair: tba | |
|---|---|
| 14:30 - 14:50 | **Martin Pichotka**, Freiburg, Germany<br>Photon-counting detectors in pre-clinical & mCT – benefits and challenges |
| 14:50 - 15:10 | **Astrid Wietelmann**,Bad Nauheim, Germany<br>$T_1$ determination with rapid 2D Gradient Echo Imaging also applicable in cardiac MRI |
| 15:10 - 15:30 | **Joanes Grandjean**, Nijmegen, The Netherlands<br>Animal Imagers Unite! Lessons learned from working together and path forward |
| 15:30 - 15:50 | **Marian Cholewa**, Rzeszów, Poland<br>Application of a deep learning-based analysis in magnetic resonance elastography (MRE) |
| 15:50 - 16:10 | **Jochen Franke**, Ettlingen, Germany<br>Magnetic Particle Imaging – one fascinating pillar of Bruker's multimodal life science portfolio |
| 16:10 - 17:00 | **Claudia Oerther**, Ettlingen, Germany<br>Ensuring data quality, reliability, and reproducibility through Quality Assurance Procedures in Preclinical in (PET)/MR |

| | |
|---|---|
| 16:30- 17:00 | Coffee Break |

| | |
|---|---|
| 17:00- 18:30 | Poster Session |

| | |
|---|---|
| 18:30 | Transfer to the City Centre, |

| | |
|---|---|
| 19:00- 21:00 | Conference Dinner, Krupnicza street |

**Wednesday, December 6 IFJ PAN, Main Building, Auditorium**

| 7. Young researchers also have a voice; Chair: tba | |
|---|---|
| 9:00 - 9:10 | **Karen Contreras-Muñoz**, Leioa, Spain<br>Design of Smart Nanoprobes for $^{19}$F-MRI Detection of MMP-2/9 in Stroke, |
| 9:10 - 9:20 | **Alvja Mali**, Wageningen, The Netherlands<br>Perfluorocarbon-PLGA particle ultrastructure affects pH sensitivity in $^{19}$F NMR and MRI |
| 9:20 - 9:30 | **Natalia Jirát-Ziółkowska**, Prague, Czech Republic<br>Biocompatible Polymer for Real-Time ROS-triggered changes in $^{31}$P-MR and optical imaging |
| 9:30 - 9:40 | **Nicolas Stumpe**, Düsseldorf, Germany<br>Non-invasive determination of oxygen partial pressure in ischemic tissue by $^{19}$F MR relaxometry |
| 9:40 - 9:50 | **Felix Schoknecht**, Berlin, Germany,<br>$^{19}$F Magnetic Resonance Imaging in Experimental Subarachnoid Hemorrhage |

| | |
|---|---|
| 9:50 - 10:00 | **Silvester J. Bartsch**, Vienna, Austria<br>Correlative multimodal biomarker identification of three breast cancer molecular subtypes: From image acquisition to machine-learning-based radiomics |
| 10:00 - 10:10 | **Kamil Lipiński**, Warsaw, Poland,<br>Evaluation of Intra Voxel Incoherent Motion (IVIM) methodology in the context of perfusion clinical protocols |
| 10:10 - 10:20 | **Zofia Schneider**, Kraków, Poland<br>DTI reveals age-related changes in brain gray matter in healthy young to middle-aged adults |
| 10:20 - 10:30 | ~~**Anna K. Stefańska**, Kraków, Poland,~~ (WITHDROWN)<br>~~DTI studies of the Multiple Sclerosis influence on the Uncinate Fasciculus structure using the BSD-DTI~~ |

| | |
|---|---|
| 10:30 - 11:00 | Coffee Break, IFJ cantine |

| **8. Local projects forum Chair: tba** | |
|---|---|
| 11:00 - 11:20 | **Grzegorz Kwiatkowski**, Kraków, Poland<br>Quantitative assessment of coronary vascular permeability and oxidant stress using DCE MR |
| 11:20 - 11:40 | **Barbara Błasiak**, Kraków, Poland<br>Core/shell Nanoparticles for cancer detection in animal models using 9.4T MRI system |
| 11:40 - 11:50 | **Juan Yang**, Oslo, Norway<br>Synthesis and characterization of multifunctional nanoparticles for potential theranostic applications |
| 11:50 - 12:00 | **Kamil Stachurski**, Kraków, Poland<br>Contrasting properties of hybrid nanosilica and cerium oxide nanoparticles for potential theranostic applications |

| **9. Closing** | |
|---|---|
| 12:00 - 12:15 | Closing Remarks – **Władysław Węglarz** |

| | |
|---|---|
| 12:15- 13:00 | Lunch, IFJ cantine |

| **10.Optional – A bit of local history** | |
|---|---|
| 13:00 – 18:00 | Wieliczka Salt Mine excursion |

# Spis treści

# List of Posters

| | |
|---|---|
| 1. | **Vera Flocke**, Katja Wegener, Tamara Straub, Maria Grandoch, Ulrich Flögel<br>MR-based phenotyping reveals early lipodystrophy in diet-induced obesity |
| 2. | **Anna Bar**, Brygida Marczyk, Anna Grochot-Przęczek, Stefan Chłopicki<br>MRI-based in vivo detection of the early changes in vascular phenotype in murine models |
| 3. | **Barbara Sitek**, Anna Bar, Stefan Chłopicki<br>Resolution of endothelial dysfunction in the course of endotoxemia in young and aged mice measured by MRI in vivo |
| 4. | **Zofia Schneider**, Agnieszka Słowik, Artur T. Krzyżak<br>Multiple sclerosis disrupts natural age-related changes in the brain - a DTI study |
| 5. | **David Červený**, Zuzana Berková, František Saudek, Kateřina Sulková, Dominik Havlíček, Vilém Neděla, Daniel Jirák<br>Visualisation of Pancreatic Islets transplanted into the greater omentum using an ECM skeleton as a supportive structure |
| 6. | **Nicolas Stumpe**, Tuba Güden-Silber, Rebekka Schneckmann, Katharina Wolters, Maria Grandoch, Ulrich Flögel<br>Non-invasive determination of oxygen partial pressure in ischemic tissue by $^{19}$F MR relaxometry |
| 7. | **Pia Pötschner**, Anja Nitzsche, Felix Schoknecht, Philipp Boehm-Sturm, Peter Vajkoczy, Ran Xu<br>PFCE in CX3Cr1 mice with Chronic Cranial Window after experimental Subarachnoid Hemorrhage |
| 8. | Armita Dash, Fong-Yu Cheng, Krzysztof Jasinski, David MacDonald, Boguslaw Tomanek, Frank C. J. M. van Veggel, **Barbara Blasiak**<br>Molecular Magnetic Resonance Imaging of Prostate Cancer using Targeted Core/Shell Nanoparticles |
| 9. | David MacDonald, Armita Dash, Frank C.J.M.van Veggel, BoguslawTomanek, **Barbara Błasiak**<br>Contrast Enhancement in MRI Using Combined Double Action Contrast Agents and Image Post-Processing in the Breast Cancer Model |
| 10. | **Alvja Mali**, Navya U. Nayak, Jessie van Doesburg, Remco Fokkink, N. Koen van Riessen, Robbin de Kruijf, Mangala Srinivas<br>Polymeric Particles Entrapping Perfluorocarbons: A Six-Year Stability Study |
| 11. | **Dominik Havlicek**, Vyshakh M. Panakkal, Ondrej Sedlacek, Daniel Jirak<br>Fluorinated Nanoparticles as Theranostic Platform for $^{19}$F MRI |
| 12. | **Michał Wieteska**, Lucyna Matusewicz, Aleksander Czogalla, Grzegorz Domański, Piotr Bogorodzki<br>Innovative Liposomal Contrast Agent for Advanced MRI Diagnostics |
| 13. | **Natalia Łopuszyńska**, Krzysztof Szczepanowicz, Marta Szczęch, Krzysztof Jasiński, Kamil Stachurski, Katarzyna Kalita, Piotr Warszyński, Władysław P. Węglarz<br>Gadolinium labeled polyelectrolyte nanocapsules for drug delivery and MRI detection – MR investigation of the influence of shell composition on contrasting properties |
| 14. | **Natalia Łopuszyńska**, Kamil Stachurski, Terje Didriksen, Juan Yang, Anna Lind, Sacha Muller, Magdalena Regulska, Monika Leśkiewicz, Magdalena Procner, Krzysztof Jasiński, Władysław Lasoń, Piotr Warszyński, Władysław P. Węglarz<br>Contrasting properties of hybrid nanosilica and cerium oxide nanoparticles for potential theranostic applications |

| | |
|---|---|
| 15. | **Joachim Friske**, Silvester J. Bartsch, Daniela Laimer-Gruber, Thomas Wanek, Claudia Kuntner-Hannes, Thomas H. Helbich, Katja Pinker<br>Comparison of two software packages to analyze preclinical dynamic contrast-enhanced MRI data to evaluate the angiogenic status of the tumor microenvironment in a xenograft breast cancer model |
| 16. | **Monika Drabik**, Michał Wieteska, Marlena Wełniak-Kamińska, Piotr Bogorodzki<br>Methodological issues of manganese-enhanced resonance imaging (MEMRI) and practical applications |
| 17. | **Karolina Janiszewska**, Grzegorz Domański, Wojciech Obrębski, Mateusz Midura, Michał Wieteska, Piotr Bogorodzki<br>A temperature-controlled NMR head for diffusion and relaxation measurements of water solutions of superparamagnetic particles (SPM) in low field MRI scanner |
| 18. | **Sebastian Plona**, Henryk Figiel, Katarzyna Lipka, Jolanta Gawlińska<br>The impact of technical innovations on the MRI image quality |
| 19. | **Ewelina Baran**, Piotr Kulinowski<br>3D printed pharmaceutical dosage forms and wound dressings studied by MRI methods |
| 20. | **Natalina Makieieva**, Teobald Kupka, Oimachmad Rachmonov, Leszek Stobiński<br>Theoretical prediction of NMR spectra for drug delivery systems |
| 21. | **Teobald Kupka**, Natalina Makieieva, Joanna Nackiewicz, Barbara Blicharska, Magdalena Witek<br>Black and green tea from the NMR point of view |

# Oral Presentations

**Fluorine-19 Magnetic Resonance Imaging of the Lungs using Octafluorocyclobutane**

Mitchell Albert

Lakehead University/Thunder Bay Regional Research Institute, Thunder Bay, Canada

Inert fluorinated gases are promising novel inhalation agents for pulmonary functional magnetic resonance imaging (MRI)[1]. Numerous studies demonstrated the feasibility of fluorine-19 ($^{19}$F) MRI of the lungs using perfluoropropane (PFP)[2,3] and sulfur hexafluoride ($SF_6$)[4] for diagnostics and the various lung disorders investigation. High image signal-tonoise ratio (SNR) achievement is possible by a high number of signal averages allowed by short $T_1$ relaxation times. Furthermore, $^{19}$F has a high natural abundance (~100%), a large gyromagnetic ratio, and is absent naturally in the living organism. These benefits result in the maximization of the $^{19}$F MRI signal.

Despite wide utilization of PFP and $SF_6$ gases in research studies, it is feasible to explore other inert fluorinated gases that can enhance the SNR level of $^{19}$F pulmonary MRI. In this study, we explored the performance of octafluorocyclobutane (OFCB) as an inhalation agent for $^{19}$F pulmonary MRI in healthy rats[5]. OFCB contains eight chemically equivalent fluorine atoms per one molecule (which is a greater number of equivalent $^{19}$F atoms compared to other fluorinated gases) and has a longer spin-spin relaxation time. To evaluate the feasibility of OFCB as a fluorinated gas for $^{19}$F lung MRI, we conducted a comparative analysis between OFCB and the previously investigated PFP, with the aim of assessing the SNR of OFCB scans in relation to PFP scans.

*In vivo* relaxation times of OFCB-$O_2$ mixture were measured as 17.77±1.5 ms and 3.4 ± 0.4 ms for $T_1$ and $T_2^*$ respectively. Lung images acquired in axial orientation using 70$^o$ Ernst flip angle (FA) condition (TR = $T_1$) and gradient echo (GRE) pulse sequences. The average was performed over either 11s (single breath-hold) or 185 s (continuous breathing) resulting in SNR of 9.72±2.1 and 14.48±4.51 respectively. The same images acquired using PFP gas demonstrated smaller SNR of 9.72±2.0 for the same single breath-hold protocol and of 12.68±4.09 for continuous breathing. OFCB images acquired using continuous breathing protocol and full longitudinal magnetization recovery condition (FA = 90$^o$, TR = 5$T_1$) showed the SNR equal to 10.23±0.7, whereas PFP images acquired using the protocol demonstrated lower SNR of 8.81±0.46.

OFCB significantly outperformed PFP in all three different imaging protocols ($p < 0.05$). The observed normalized SNR (normalized for the number of signal averages) advantage of OFCB agreed well with theoretical predictions for single breath-hold protocol and for continuous breathing with 90$^o$ excitation FA. The SNR of OFCB was up to 21% higher compared to the PFP scans. A slight deviation from theoretical values was observed in the continuous breathing protocol with 70$^o$ Ernst angle, potentially due to a minor mismatch between the OFCB $T_1$ *in vivo* and the TR value used during the scan. In addition, the absence of respiratory gating could explain this discrepancy. In general, OFCB shows a considerable performance advantage over PFP, resulting in notably superior image quality in OFCB scans.

References:

1. Couch, M. J. *et al.* $^{19}$F MRI of the Lungs Using Inert Fluorinated Gases: Challenges and New Developments. *J. Magn. Reson. Imaging* **49**, 343–354 (2018).
2. Neal, M. A., Pippard, B. J., Simpson, A. J. & Thelwall, P. E. Dynamic susceptibility contrast $^{19}$F-MRI of inhaled perfluoropropane: a novel approach to combined pulmonary ventilation and perfusion imaging. *Magn. Reson. Med.* **83**, 452–461 (2020).
3. Obert, A. J. *et al.* $^1$H-guided reconstruction of $^{19}$F gas MRI in COPD patients. *Magn. Reson.Med.* **84**, 1336–1346 (2020).

**Pivotal role of the protein corona on NP cellular uptake for boosting $^{19}$F-MRI sensitivity**

Francesca Baldelli Bombelli

Department of Chemistry, Politecnico di Milano, Italy

The success of $^{19}$F-MRI for tracking of therapeutic cells leverages on the development of

highly performant $^{19}$F-probes. PLGA-based NPs containing PERFECTA, a multibranched, superfluorinated molecule with an optimal MRI profile thanks to its 36 magnetically equivalent fluorine atoms, are promising $^{19}$F-MRI probes. In this contribution the importance of NP surface functionalization in relation to NP interactions with the biological environment will be shown, stressing the pivotal role played by the protein corona (PC) on cellular labelling efficacy. The formation of PC NP in a cell culture medium is the key element for the optimization of cell labelling and can be exploited to boost NP cellular uptake with a considerable increase of the detection sensitivity by $^{19}$F-MRI.

**Multicolored-MRI reporter genes - WITHDROWN**

Amnon Bar-Shir

Weizmann Institute of Science, Rehovot, Israel

Recent advances in tissue clarification[1] enabled 3D multiplexed mapping of genetically engineered reporters in excised organs postmortem. Yet this approach is not applicable to noninvasive in vivo studies of dynamic and complex cellular events. Reporter genes developed for MRI present an alternative solution for in vivo mapping of transgene expression. However, MRI reporter genes are limited in possessing the multiplex imaging capabilities needed for the simultaneous “illumination” of cellular processes. Moreover, a major pitfall for advanced developments of MRI reporter genes is the low-throughput capabilities of MRI-guided screening preclude the large-scale mutagenesis campaigns that have served so well in engineering fluorescent proteins.[2] Here, we capitalized on the frequency encodability CEST MRI to obtain MRI-based colors,[3] combined with an

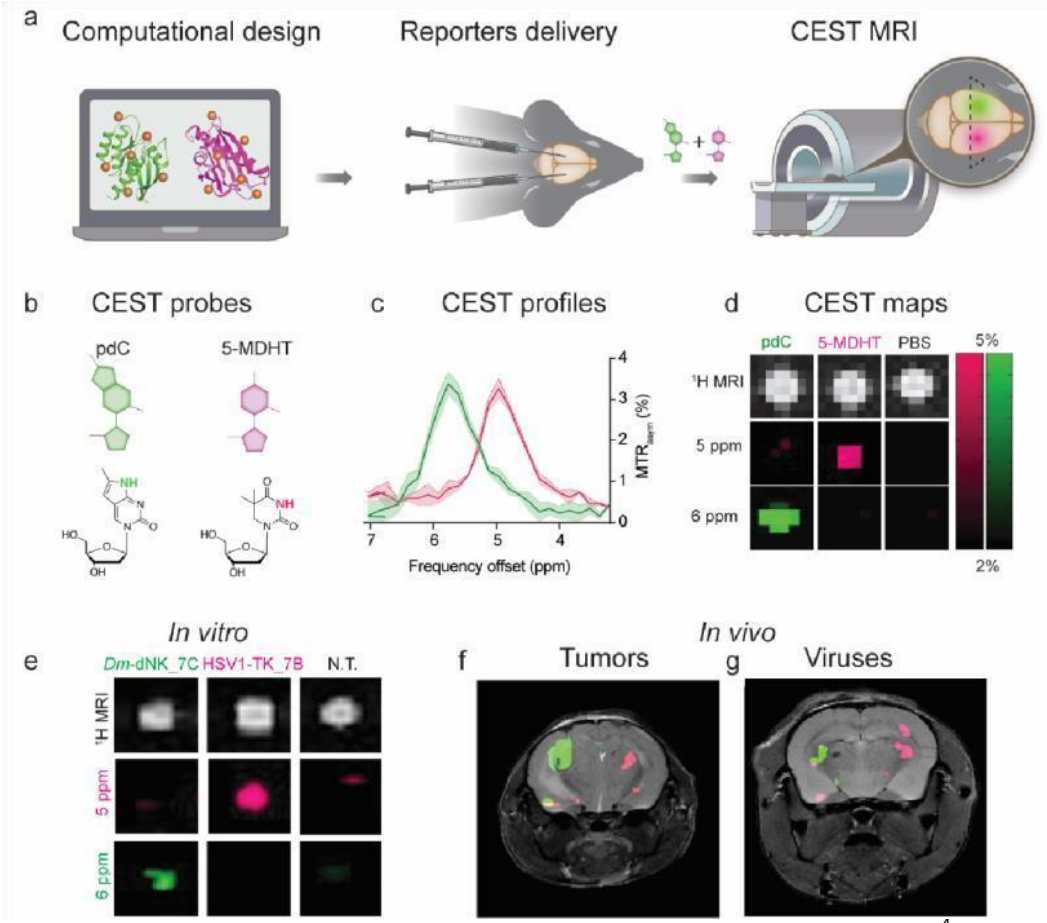


automated and computational evolution-based protein design method (PROSS)[4] to design fully orthogonal genetically engineered MRI reporter genes.[5] We demonstrated the implementation of the genetically encoded reporter system, which enables MRI mapping of transgenes expression in a pseudo-multi-color fashion. Our approach extends the

"multicolor" toolbox to thus far inaccessible deep tissues in live subjects. Our work demonstrates that new protein-design methods can be applied to systems that are recalcitrant to conventional high-throughput screening in order to generate highly desirable properties.

References:
1. Chung, K. et al. Structural and molecular interrogation of intact biological systems. Nature 497, 332-337 (2013).
2. Shaner, N.C. et al. Improved monomeric red, orange and yellow fluorescent proteins derived from Discosoma sp. red fluorescent protein. Nat Biotechnol 22, 1567-1572 (2004).
3. McMahon, M.T. et al. New "multicolor" polypeptide diamagnetic chemical exchange saturation transfer (DIACEST) contrast agents for MRI. Magn Reson Med 60, 803-812 (2008).
4. Goldenzweig, A. et al. Automated Structure- and Sequence-Based Design of Proteins for High Bacterial Expression and Stability. Mol Cell 63, 337-346 (2016).
5. Allouche-Arnon, H. et al. Computationally designed dual-color MRI reporters for noninvasive imaging of transgene expression. Nat Biotechnol (2022).

**Core/shell Nanoparticles for cancer detection in animal models using 9.4T MRI system**

Barbara Blasiak[1,2], Frank C. J. M. van Veggel[3], Armita Dash[3], Boguslaw Tomanek[1,2,4]

[1]Polish Academy of Sciences, Institute of Nuclear Physics, Krakow, Poland; [2]Department of Clinical Neurosciences, University of Calgary; Calgary, Canada; [3]Department of Chemistry, University of Victoria, Victoria, Canada; [4]University of Alberta, Department of Oncology, Edmonton, Canada

Magnetic Resonance Imaging (MRI) has been used for early cancer detection, as it provides high spatial resolution and soft tissue contrast. Yet its specificity is low. Standard contrast enhanced MRI is based on tumors vasculature (i.e. Gd-based) and it does not provide sufficiently high specificity for tumor diagnosis and thus targeted contrast agents providing $T_2$ contrast have been applied to provide information on tumor specificity[1,2].

Therefore, we have developed core/shell NaDyF4/NaGdF4 nanoparticles changing both $T_1$ and $T_2$ relaxation times of surrounding water molecules. The NPs were conjugated with tumor specific antibodies and proteins. The relaxation times ($T_1$ and $T_2$) of the nanoparticles with various core/shell sizes and concentrations were measured at 9.4T and 3T to find the optimum $T_1/T_2$ ratio for maximum contrast. $T_1$- and $T_2$-weighted images using core/shell nanoparticles of the animal models of brain, breast and prostate cancer were collected. Mouse models of cancer were used at 9.4T. We imaged 6 weeks nude mice with the tumor before the injection of the targeted and non-targeted contrast agents and in different time after injection (10 min after,1h, 2h and 24h). The core/shell based NPs provided improved tumor contrast when the $T_1$ and $T_2$-weighted MR pulse sequences were applied. The results show that the developed NPs may improve the efficacy of MRI in cancer detection.

References:
1. Blasiak B, Tomanek B, et al Detection of $T_2$ changes in an early mouse brain tumor. Mag Res Imag 2010, 28:784-9.
2. Tomanek B, Iqbal U, Blasiak B, at al. Evaluation of Brain Tumor Vessels Specific Contrast Agents for Glioblastoma Imaging. Neuro-Oncology, 2012, 14(1):53-63.

**A no brainer? $^{19}$F MR neuroimaging of cerebrovascular disease - WITHDROWN**

Philipp Boehm-Sturm

Charité 3$^{R}$ - Replace | Reduce | Refine, Center for Stroke Research Berlin and Dpt. of experimental Neurology, Charité – Universitätsmedizin Berlin, Berlin, Germany

The sensitivity of $^{19}$F MRI has dramatically improved with higher field strengths, improved coil technology and sophisticated acquisition and reconstruction strategies. One research field that has particularly profited from these improvements is preclinical $^{19}$F MR neuroimaging in cerebrovascular disease, for which the small size of the rodent brain and hurdles to achieve higher concentrations of external tracers have previously presented major challenges. In my overview talk I will summarize our work on (i) stem cell tracking in murine ischemic stroke [1], (ii) $^{19}$F oxygenation imaging in murine vascular dementia [2], (iii) in vitro development of calcium-responsive $^{19}$F probes [3] and (iv) an ongoing study on $^{19}$F

MRI of inflammation in murine subarachnoid hemorrhage.

References:
[1] P. Boehm-Sturm *et al.*, "A multi-modality platform to image stem cell graft survival in the naïve and stroke-damaged mouse brain," *Biomaterials,* vol. 35, no. 7, pp. 22182226, 2014/02// 2014, doi: 10.1016/j.biomaterials.2013.11.085.
[2] A. A. Khalil *et al.*, "Longitudinal $^{19}$F magnetic resonance imaging of brain oxygenation in a mouse model of vascular cognitive impairment using a cryogenic radiofrequency coil," *Magnetic Resonance Materials in Physics, Biology and Medicine,* vol. 32, no. 1, pp. 105-114, 2019/02/14/ 2019, doi: 10.1007/s10334-0180712-x.
[3] P. Kadjane *et al.*, "Dual-Frequency Calcium-Responsive MRI Agents," *Chemistry – A European Journal,* vol. 20, no. 24, pp. 7351-7362, 2014/06/10/ 2014, doi: 10.1002/chem. 201400159.

**$^{1}$H NMR-based metabolomics in head and neck cancer treatment – whether it may be helpful for a clinician?**

Łukasz Boguszewicz, Agata Bieleń, Mateusz Ciszek, Agnieszka Skorupa, Krzysztof Składowski, Maria Sokół

Maria Sklodowska-Curie National Research Institute of Oncology, Gliwice Branch, 44-102 Gliwice, Poland

Head and neck cancers (HNC) develop in organs crucial for respiratory, nutritional, and social functions. The standard organ preservation treatment methods for HNC are sequential and/or concurrent radiotherapy (RT) and chemotherapy (CHT). Intensified treatment modalities improved the survival of patients with HNC, but are associated with significant temporary or permanent toxic side effects in normal tissue and/or involved regions (acute radiation sequelae, ARS). The metabolic composition of blood is known to reflect the response of organisms to disease as well as treatment-related and environmental factors. $^{1}$H NMR-based serum metabolomics has been used to investigate the molecular response to anticancer treatment, with particular emphasis on its toxicity. We were able to identify metabolic alterations characteristic of the direct response to RT/CHT and secondary effects resulting from treatment-induced toxicity. The obtained results not only constitute the basis for further research on personalized medicine but also show potential for future use in clinical practice.

**MRI in the common Marmoset - Bridge on the way from mouse to human.**

Susann Boretius

Functional Imaging Laboratory, Leibniz Institute for Primate Research, Göttingen, Germany

**Real-Time In Vivo MPI Cytometry**

Jeff W.M. Bulte

The Johns Hopkins University School of Medicine, Department of Radiology and Radiological Science Baltimore, USA

Magnetic particle imaging (MPI) has emerged as non-invasive imaging modality that can be applied for in vivo (stem) cell tracking[1]. It can use the same SPIO nanoparticles as those used with MRI, but instead of MRI contrast agents, these formulations act as MPI tracer agents to provide “hot spot” signal without tissue background signal and true cell quantification[2], enabling “in vivo cytometry” on a time scale of minutes. Examples will be shown for mesenchymal stem cells (MSCs) and neural precursor cells (NPCs) after intra-arterial injection in mouse models. Using fiducials with known cell concentrations, the cytometric ratio of the number of cells localizing in the liver/lung vs. the brain differed 10-fold between the two cell types, representing the different cellular volumes which is a critical parameter for passage through the cerebral capillary network.
By virtue of their tumor-tropism, MSCs can also be applied as cellular theranostics to deliver

and retain theranostic gold-containing SPIOs to tumors. Using in vivo MPI cytometry of intratumoral vs. systemic distribution of gold-SPIO-loaded MSCs, we found that the total amount of tumor-associated particles different 10-fold between labelled hMSCs and “naked” nanoparticles, which correlated with the efficacy of laser irradiation-mediated photothermal therapy (PTT) for eradication of tumors.

Finally, we are developing an all-in-one nanotheranostic plastform that can be visualized with MRI, MPI, CT, and photoacoustic imaging. The formulation contains albumin, bismuth sulfide, and SPIO and can act as a radiosensitizer and activator for PTT and magnetic hyperthermia. Examples of in vivo MPI cytometry will be shown for stem cells directly implanted in the brain, and how MPI cytometry compares to cell quantification with CT and MRI.

References:
1. Bulte, JWM et al., *Tomography* **2015**, 1, 91-97.
2. Bulte, JWM et al., *Adv. Drug Del. Rev*. **2019**, 138, 293-301.

**Water Dispersible Small Nanoparticles with Fluorinated Surface and High Relaxation Times for $^{19}$F MR Applications - WITHDROWN**

Monica Carril

Instituto Biofisika (CSIC, UPV/EHU), Leioa, Bizkaia, Spain. Departamento de Bioquímica y Biología Molecular, UPV/EHU, Leioa, Bizkaia, Spain. Ikerbasque, Basque Foundation for Science, Bilbao, Spain.

The synthesis of fluorinated nanoparticles for $^{19}$F MRI with fluorine exposed on the surface is challenging due to solubility issues associated to the intrinsic hydrophobicity of fluorine. For this reason, fluorinated probes are usually encapsulated in liposome-type nanostructures which may have stability issues, a size that limits some *in vivo* applications, and the encapsulation may affect negatively the relaxation times of fluorine.

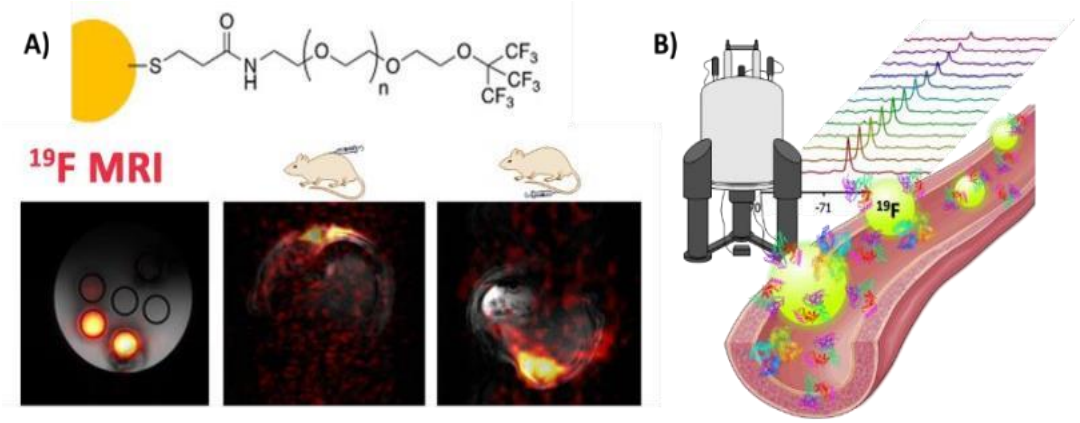


Figure 1. A) Fluorinated NPs and $^{19}$F MRI images. B) $^{19}$F NMR diffusion measurements

In this sense, small nanoparticles (NPs) with fluorinated PEG ligands may be of interest. Our design relies on the small size of the core (< 4 nm) and the flexibility and water solubility of PEG linkers used to bind fluorine to the NP surface, which allows for very high $T_2$ values (1 s), reasonable $T_1$ values (1.2 s) and a high local concentration of equivalent fluorine atoms (1300 atoms/NP), while keeping the colloidal stability in water.[1] We present two methods to fluorinate the surface of NPs, maintaining $T_2$ values from 0.5 to 1 s. Such NPs have been successfully detected by *in vivo* $^{19}$F MRS and $^{19}$F MRI.[1b] Interestingly, the small size of such fluorinated NPs allowed us to study protein corona formation by NP size analysis in the presence of proteins by $^{19}$F NMR diffusion measurements.[2] By using our method, we observed that the presence of fluorine on the surface of NPs apparently did not provoke unwanted adhesion of proteins.[2a]

References:
1. Michelena O. *et al. Chem. Commun.* **2017**, *53*, 2447. b) Arango J.M. *et al. ACS Appl. Mater.*

*Interfaces* **2021**, *13*, 12941.
2. Carril M. *et al. Nat. Commun*. **2017**, *8*, 1542. b) Padro D. *et al. Small* **2020**, *36*, 2001160.

**(MRE)**

Marian Cholewa[1], Vitaliy Atamaniuk[1], Andrii Pozaruk[1], Łukasz Hańczyk[2], Marzanna Obrzut[2], Bogdan Obrzut[2], Krzysztof Gutkowski[2]

[1]Institute of Physics, College of Natural Sciences, University of Rzeszow, Poland; [2]College of Medical Sciences, University of Rzeszow, Poland

**Background:** Magnetic Resonance Elastography (MRE) is an emerging imaging technique that allows for non-invasive quantitative assessment of various biophysical parameters in human tissue, such as viscosity and stiffness. Despite its potential, MRE, in comparison to conventional imaging methods like ultrasound or magnetic resonance imaging, faces several challenges, including manual evaluation through the drawing of regions of interest. Manual assessment of MRE data is susceptible to low intra- and inter-rater reliability and is time-consuming. Moreover, MRE exams can be affected by patient motion due to breathing or shifting. In this study, we explore the utility of deep learning-based methods for MRE data analysis and enhancement.

**Methods:** Deep learning methods have gained significant attention in recent years for biomedical image analysis. We conducted an extensive literature review to identify prior work on the application of deep learning in MRE. We tested similar approaches on MRE data collected in our laboratory, utilizing deep learning for tasks such as image enhancement and exam interpretation.

**Results:** Aldoj et al. employed deep learning to automate the quantification of biomechanical tissue parameters in prostate MRE, achieving performance comparable to human readers and enabling automated quantification of tissue viscoelasticity [1]. Pollack et al. developed a deep learning-based model capable of predicting liver stiffness using conventional MRI images, which may enhance result reliability assurance [2]. Shan et al. explored the feasibility of accelerating MRE using deep learning and demonstrated its potential for rapid MRE acquisition [3]. Our team also developed and tested deep learning-based algorithms for automated image segmentation and patient motion reduction. Our algorithms automatically delineate the region of interest (with a dice score of approximately 0.7) and generate motion-free images with an approximately 30% relative error compared to ground truth images.

**Conclusions:** Deep learning proves to be a robust tool for biomedical image analysis, encompassing tasks like region of interest segmentation, image assessment, and quality enhancement. However, although deep learning shows promise in various aspects of MRE, further development is necessary for its full integration into clinical practice.

References:
1. Aldoj, N., Biavati, F., Dewey, M. et al. Sci Rep 12, 2001 (2022). doi: 10.1038/s41598-022-05878-5.
2. Pollack BL, Batmanghelich K, Cai SS, Gordon E, Wallace S, Catania R, Morillo-Hernandez C, Furlan A, Borhani AA. Radiol Artif Intell. 2021 Sep 29;3(6):e200274. doi: 10.1148/ryai.2021200274.
3. Shan X, Yang J, Xu P, Hu L, Ge H. Med Phys. 2022 Mar;49(3):1803-1813. doi: 10.1002/mp.15471.

**Detection of inflammatory cell migration using MRI**

Cornelius Faber

Translational Research Imaging Center (TRIC), University of Münster, Münster, Germany

MRI is capable of image resolution below 0.1 mm pixel size. However, for cellular MRI, this dimension is not sufficient to directly resolve individual cells in vivo. Indirect imaging strategies are therefore required to detect individual immune cells and visualise their migration in the body. Successful strategies involve labelling target cells with either directly detected imaging agents, such as $^{19}$F-containing compounds, or indirectly detected contrast

agents, such as iron oxide nanoparticles (IONPs). The latter allows the detection of single cells and the use of time-lapse MRI for real-time tracking of immune cells in the healthy animal as well as during the onset and progression of inflammation. We have applied time-lapse MRI to several mouse models of disease and have shown that time-lapse MRI of immune cells in the brain can indicate the immune status of the body. We have further developed methods to perform accelerated time-lapse MRI to capture the migration of faster (than patrolling) moving cells within the vasculature.

In more severe inflammation, and also in the tumour microenvironment (TME), massive immune cell infiltration occurs and single cell tracking is not required. MRI techniques that are sensitive to microstructural changes are well-suited to resolve cellular infiltration. We have used time-dependent diffusion MRI with oscillating gradients to characterise cellular microstructure in the TME. Our approach is able to distinguish between macrophage and T-cell infiltration. It is therefore suitable for differentiating tumours of different malignancies and also allows characterization of tumour response as early as three days after initiation of therapy before any changes in tumour size can be detected.

References:

1. Masthoff M, Gran S, Zhang X, Wachsmuth L, Bietenbeck M, Helfen A, Heindel W, Sorokin L, Roth J, Eisenblatter M, Wildgruber M, Faber C. Temporal window for detection of inflammatory disease using dynamic cell tracking with time-lapse MRI. Sci Rep 2018;8: 9563.
2. Masthoff M, Freppon FN, Zondler L, Wilken E, Wachsmuth L, Niemann S, Schwarz C, Fredrich I, Havlas A, Block H, Gerwing M, Helfen A, Heindel W, Zarbock A, Wildgruber M, Faber C. Resolving immune cells with patrolling behaviour by magnetic resonance time-lapse single cell tracking. EBioMedicine 2021;73: 103670.
3. Armstrong M, Wilken E, Freppon F, Masthoff M, Faber C, Xiao D. Dynamic cell tracking using time-lapse MRI with variable temporal resolution Cartesian sampling. Magn Reson Med 2023;90: 2443-2453.
4. Hoffmann E, Gerwing M, Niland S, Niehoff R, Masthoff M, Geyer C, Wachsmuth L, Wilken E, Höltke C, Heindel WL, Hörr V, Schinner R, Berger P, Vogl T, Eble JA, Maus B, Helfen A, Wildgruber M, Faber C. Profiling specific cell populations within the inflammatory tumor microenvironment by oscillating-gradient diffusion-weighted MRI. J Immunother Canc 2023;11: e006092.

**Molecular Imaging via $^{19}$F MRI**

Ulrich Flögel

Experimental Cardiovascular Imaging, Institute for Molecular Imaging, Heinrich Heine University, Düsseldorf, Germany

Among preclinical molecular imaging approaches, fluorine ($^{19}$F) MRI has recently attracted great interest from the biomedical research community due to the special properties of fluorinated materials and the $^{19}$F nucleus. Fluorine is the most sensitive nucleus for MRI besides hydrogen, but is present in the body only in insignificant amounts, allowing background-free detection of fluorinated substances as 'hotspots' by combined $^{1}$H/$^{19}$F MRI and making fluorine-containing molecules ideal tracers for a wide range of MRI applications. In addition, there exists a well-characterized class of compounds – perfluorocarbons – that have very high fluorine content and are both biochemically and physiologically inert. Creative molecular design also allows the MR properties (especially chemical shift and relaxation times) of these compounds to be made 'responsive' to changing environmental conditions (such as pH, $PO_2$, enzyme activations, etc.) and thus used for their readout. The talk will focus on recent advances in $^{19}$F MRI with special emphasis on cardiovascular disease models and will span a very interdisciplinary field – from chemistry to synthesize specific probes to biomedical applications as well as physics for optimizing data acquisition and processing to further increase sensitivity and specificity.

**Magnetic Particle Imaging - one fascinating pillar of Bruker's multimodal life science portfolio**

Jochen Franke

Bruker Biospin, Ettlingen, Germany

Preclinical imaging plays an important role in the understanding of biological processes in healthy and diseased states as well as responses to pharmacological, physiological or environmental challenges. A comprehensive understanding of biological systems through the use of state-of-the-art analytical technologies can significantly advance clinical diagnosis and therapy routines.

Bruker BioSpin is a renowned provider of advanced imaging technologies ranging from Magnetic Resonance Imaging (MRI), Computed Tomography (CT), Positron Emission Tomography (PET), Single Photon Emission Computed Tomography (SPECT) to the latest imaging technology, Magnetic Particle Imaging (MPI). With our mission to develop each imaging technology to its best, Bruker drives innovation in new methods and solutions for scientists, enabling groundbreaking discoveries. Our instruments enable critical assessments of healthy and diseased mechanisms at the organ, tissue, cellular and molecular levels. Preclinical imaging is also central to evaluating the efficacy and safety of new treatments and quantification of the drug’s biodistribution prior to clinical use. That is why Bruker continues to invest in innovation and new technologies.

We seamlessly combine multiple imaging technologies in multimodal, easy-to-use instruments for head-to-toe investigations in your research. Best-in-class hardware and software packages provide streamlined workflows from animal handling to morphological and functional data acquisition to image reconstruction and post-processing. This includes quantification and visualization tools for various biomedical imaging applications.

Through numerous collaborations with leading research centers and our dynamic development teams, Bruker invests in the advancement of Magnetic Particle Imaging in the preclinical area, paving the way for translational and clinical perspectives. The use of nanomaterials and their specific response to external magnetic fields is not only crucial for molecular imaging, but also opens the door to the development of novel theranostic strategies, which in turn can improve patient outcomes and save lives.

This talk will present the basic principle of signal generation and the spatial encoding schemes employed by MPI. The wide range of applications of MPI will be demonstrated by presenting the research results of our customers. Taking advantage of MPI as the basis for a theranostic platform, the vision for future MPI instrumentation will round off the content. Furthermore, a high-level perspective on Bruker's multimodal preclinical imaging portfolio will be presented.

Be inspired by the recent achievements of our outstanding MPI community in the life sciences and join us in taking molecular imaging to the next level.

**Animal Imagers Unite! Lessons learned from working together and path forward**

Joanes Grandjean

Donders Institute for Brain, Behaviour, and Cognition, Nijmegen, The Netherlands. Department of Medical Imaging, Radboud University Medical Center, PO Box 9101, Nijmegen, The Netherlands

How to best acquire rodent preclinical functional MRI data? Every laboratory has an opinion on this, but are they truly objective? It has become apparent that we work with different data quality, with different potentials to capture functional connectivity phenomena, and these discrepancies cannot only be linked to preprocessing differences and analysis schemes. In this paper, I describe our community effort to describe dataset performance, identify potential best practices, and test them out in laboratory conditions. Along the way, I describe the conceptual and software advances that we brought to the table to make this project work.

**Cardiac CEST MRI to identify myocardial infarction**

Verena Hoerr

University Hospital Bonn, Bonn, Germany

**Functional X-nuclei Magnetic Resonance (Reactive Oxygen Species Detection)**

Daniel Jirak

Department of Diagnostic and Interventional Radiology, MR UnitInstitute for Clinical and Experimental Medicine, Prague, Czech Republic

In the realm of preclinical molecular imaging techniques, there has been a notable surge in interest among the biomedical research community in the field of fluorine ($^{19}F$) magnetic resonance imaging (MRI). This growing interest is primarily driven by the exceptional properties of fluorinated materials [1]. A standout feature of this method is its remarkable specificity, owing to the negligible presence of natural fluorine in the human body. This characteristic empowers the visualization of 'hotspot' signals, valuable for various biomedical applications like monitoring transplanted cells. Additionally, recent introductions of probes for phosphorous $^{31}P$ MRI [2,3,4], noted for their significant biocompatibility, have further broadened the horizons of X-nuclei MRI applications.

Some X-nuclei MRI probes, constructed with hydrophilic polymers, can facilitate functional imaging. Their responsiveness to physiological conditions allows real-time functional imaging. When combined $^{31}P/^{19}F$ MR, these probes provide complementary information critical for a comprehensive interpretation of results. We demonstrate a $^{31}P/^{19}F$ polymer probe designed for detecting reactive oxygen species (ROS), frequently abundant in pathological conditions such as cancer, that exhibits distinct phosphorous resonance frequencies in the presence and absence of ROS. This chemical shift in $^{31}P$ MR spectra is detectable even under magnetic field strengths comparable to clinical settings.

For precise in vivo localization of the probe, an inert trifluoromethyl group, unresponsive to physiological variations, is integrated into the probe's structure. This facilitates visualization through "hotspot" $^{19}F$ MR imaging and serves as an on-site reference. This approach represents an innovative paradigm in functional $^{31}P$ MR, supplementing the traditional anatomical information offered by $^{1}H$ MRI with insights into tumor physiology.

Acknowledgements:
Financial support from the Ministry of Health CR-DRO (Institute for Clinical and Experimental Medicine IKEM, IN00023001) and from the project National Institute for Research of Metabolic and Cardiovascular Diseases (Programme EXCELES, Project no. LX22NPO5104) - Funded by the European Union - Next Generation EU.

References:

1. D. Jirak, A. Galisova, K. Kolouchova, D. Babuka, M. Hruby, Magn Reson Mater Phy 2019, 32, 173.
2. N. Ziółkowska, M. Vít, R. Laga, D. Jirák, Sci. Rep. 2022, 12, 118.
3. L. Kracíková, N. Ziółkowska, L. Androvič, I. Klimánková, D. Červený, M. Vít, P. Pompach, R. Konefał, O. Janoušková, M. Hruby, D. Jirák, R. Laga, Macromol. Biosci. 2022, 22, 2100523.
4. T. Rheinberger, U. Flögel, O. Koshkina, F.R. Wurm, Commun Chem. 2023 Sep 1;6(1):182.

**Perfusion MRI on small animals beyond $K^{trans}$**

Radovan Jiřík

Institute of Scientific Instruments, Czech Academy of Sciences, Brno, Czech Republic

This contribution is focused on perfusion MRI on small animals using Dynamic Contrast-Enhanced (DCE) MRI, an experimental method used mostly in oncology for tumor diagnosis and monitoring of the treatment. It provides estimates of perfusion parameters quantifying the microvascular structure and function. DCE-MRI is based on intravenous administration of a contrast agent (CA) and $T_1$-weighted MRI of its temporal and spatial distribution. The acquired image sequence is converted to CA concentration curves in regions of interest

(e.g. tumor voxels) and fitted by a pharmacokinetic (PK) model [1].

The basic and mostly used PK models, such as the Tofts and extended Tofts models [1], are the 1st-generation models, providing estimates of the volume transfer constant, $K^{trans}$, related to blood plasma flow, $F_p$, and permeability-surface-area product, *PS* (quantifying the capillary-wall leakiness).

However, to distinguish between the effect of $F_p$ and *PS* on $K^{trans}$, more complicated so-called 2nd-generation PK models have to be used. These models require higher temporal resolution of the acquired image sequence (approx. 1 s per frame). To cover for example a 3D volume of a tumor, modern accelerated MRI techniques must be used. We have implemented a sparse radial k-space sampling method Golden-Angle Stack of Stars (GA SOS) based on spoiled gradient echo [2] on a 9.4T MR scanner Bruker Biospin (Ettlingen, Germany). For image-sequence reconstruction we use compressed-sensing reconstruction based on total variation (TV) [3] and our modifications of the low-rank plus sparse (L+S) model [4]. We are also developing a physics-based deep-learning (DL) image reconstruction – implemented as an unrolled L+S algorithm.

An important part of the PK model-fitting problem is knowledge of the arterial input function (AIF), often measured in a large artery. Measuring an AIF is difficult in small-animal DCE-MRI due to the small size of the arteries and limited spatial resolution. Instead, we propose use of blind deconvolution for estimation of the AIF indirectly from the tissue curves [5], possibly made more robust by use of TV spatial regularization [6]. Also, the PK model-fitting problem can be made more reliable by fitting the whole region-of-interest at once with induced spatial regularization [7], instead of fitting the CA concentration curves of each voxel separately.

We illustrate these approaches on DCE-MRI examinations of tumor-bearing mice and on healthy animals where the blood brain barrier (BBB) has been locally transiently opened by focused ultrasound. A realistic DCE-MRI simulator will be presented as an evaluation tool as well.

References:

1. S.P. Sourbron, D.L. Buckley, NMR Biomed. 26(8), 2013, 1004-1027.
2. L. Feng et al., MRM 72(3), 2014, 707–717.
3. J. Mendes et al., MRM 83(6), 2019, 1949–1963.
4. M. Mangová (Daňková): Ph.D. Thesis, Brno Univ. of Technol., 2018.
5. R. Jiřík et al., MRI 42, 2019, 46–56.
6. R. Jiřík et. al. ISMRM-ESMRMB conf. 2022, 7487.
7. M. Bartoš et al., MRM 82(6), 2019, 2257–2272.

**Modelling inhomogeneous magnetization transfer in myelin and intra-/extra-cellular water in normal and injured rat spinal cords ex vivo**

Michelle H. Lam[1,2], Andrew Yung[2], Jie Liu[3], Wolfram Tetzlaff[3], Piotr Kozlowski[1,2,3,4]

[1]Physics and Astronomy, University of British Columbia, Vancouver BC, Canada; [2]UBC MRI Research Centre, University of British Columbia, Vancouver, BC, Canada; [3]International Collaboration on Repair Discoveries, Vancouver, BC, Canada; [4]Radiology, University of British Columbia, Vancouver, BC, Canada

Myelin is an insulating layer, or sheath that forms around nerves, including those in the brain and spinal cord. It is made up of protein and fatty substances. The myelin sheaths allow electrical impulses to transmit quickly and efficiently along the nerve cells. A number of neurodegenerative diseases are caused by demyelination or traumatic damage to myelin sheaths. Thus, quantifying myelin content through in vivo imaging methods is extremely important for diagnosing demyelinating diseases and injuries to the central nervous system. Inhomogeneous magnetization transfer (ihMT) imaging and myelin water imaging (MWI) have both established themselves as myelin-specific MRI techniques. In this study, ihMT and MWI were combined to provide new insight into the myelin state following traumatic spinal cord injury in a preclinical model ex vivo.

The combined ihMT/MWI data were acquired from 9 formalin-fixed rat spinal cords:

uninjured (3), 3 weeks (3) and 8 weeks (3) post dorsal column transection injury. A bi-exponential function was used to fit the $T_2$ decays of each saturation type, to quantify the ihMT effect in the myelin water (MW) and intra-extracellular water (IEW) pools separately. Different levels of the $T_{1D}$ filtering were applied by using 11 $\tau_{switch}$ times in the ihMT part of the pulse sequence. Data was modelled with a modified four-pool model with the addition of dipolar reservoirs.

Values of the dipolar order relaxation time in myelin ($T_{1D}^{m}$) measured in this study were close to previously reported. There was a significant drop in $T_{1D}^{m}$ in the 3 weeks post-injury spinal cords in the fasciculus gracilis region, which suggests that $T_{1D}^{m}$ may be a potential marker for distinguishing functional myelin from myelin debris. More studies on a larger cohort are required to confirm this result. Additionally, modifications need to be made to the model to improve the fit of the ihMTR-IEW data points.

**Design principles and potential applications of molecular hydrazone switches for pH imaging in $^{19}$F MRI**

Tomasz Krawczyk, Dawid Janasik

Department of Chemical Organic Technology and Petrochemistry, Silesian University of Technology Krzywoustego 4, 44-100 Gliwice, Poland

Numerous substances, including polymers, perfluorocarbon emulsions, and various small molecules, have been explored for their potential as $^{19}$F contrast agents. This exploration arises from the challenge of designing suitable fluorinated contrast agents due to the absence of fluorine in soft tissues [1-2]. Hydrazone switches, in particular, hold promise as functional contrasts for $^{19}$F MRI due to their ability to undergo isomerization in response to biologically relevant external stimuli, such as pH [3]. The ease of modifying their structure, including the introduction of paramagnetic groups, opens the door to various potential applications in MRI [4-6].

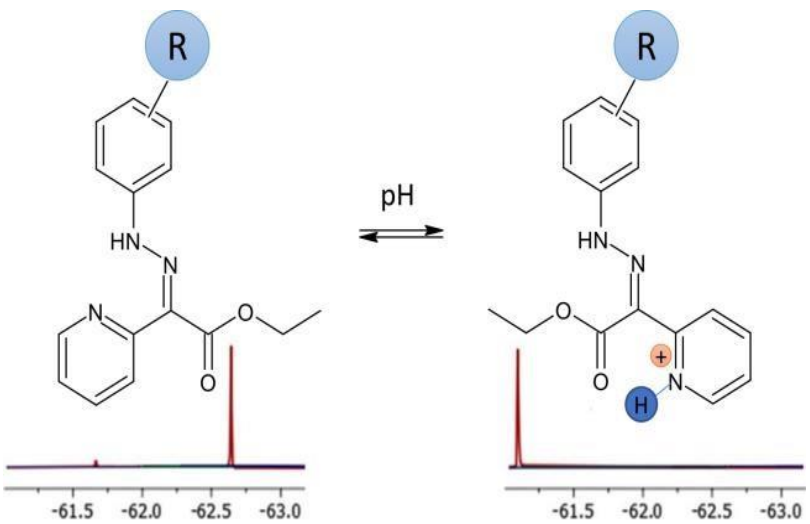


Fig. 1. Basic structure of a hydrazonate molecular switch and its $^{19}$F NMR spectrum in various environments. R = F, $CF_3$, etc."

References:

1. D. Janasik, T. Krawczyk, Chem. Eur. J., 2022, 28 art. no. e202102556.
3. M. Zalewski, D. Janasik, A. Kapała, M. Minoshima, F. Sugihara, W. Raj, J. Pietrasik, K. Kikuchi, T. Krawczyk, Macromol. Chem. Phys., 2022, 223, art. no. 2200027.
3. D. Janasik, K. Jasiński, W.P. Węglarz, I. Nemec, P. Jewula, T. Krawczyk, Anal. Chem 2022, 94, 3427.
4. D. Janasik, P. Imielska, T. Krawczyk, ACS Sens. 2023, 8, 721.
5. D. Janasik, K. Jasiński, J. Szreder, W.P. Węglarz, T. Krawczyk, ACS Sens. 2023, 8.
6. M. Zalewski, D. Janasik, A. Wierzbicka, T. Krawczyk, Inorg. Chem. 61, 19524.

**The development and characterisation of an in vivo $^{19}$F MRI imaging agent**

Robbin de Kruijf

Cenya Imaging Bv., Wageningen, The Netherlands

Our group works with polymer-entrapped perfluorocarbon (PFC) particles for in vivo imaging using $^{19}$F MRI, ultrasound, fluorescence and nuclear imaging. These particles have been spun out to a company for clinical imaging, and production at GMP grade. PFCs are simultaneously lipophobic and hydrophobic. The production process, consisting of a triphasic continuous, microfluidic system, results in particles of about 200 nm diameter with a fractal, multicore structure. We do not fully understand why small changes in the production process can result in a single or multicore internal structure. Regardless, the multicore structure has a significant biological impact, as the clearance half-life of the PFC drops nearly 15-fold with the multicore over the single core (core-shell) structure. In addition, the particles, unlike traditional (relatively fragile) gas-containing ultrasound contrast agents, are extremely stable, even for probe sonication. In addition, the internal structure impacts the $^{19}$F relaxation when paramagnetic Gd is included.

We have applied these particles to tracking various cell types in vitro and in vivo in a range of disease models, in a longitudinal and quantitative manner, and are approved for a clinical trial in the Netherlands.

**Quantitative assessment of coronary vascular permeability and oxidant stress using DCE MRI**

Grzegorz Kwiatkowski[1], Stefan Chłopicki[1,2]

[1]Jagiellonian University, Jagiellonian Centre for Experimental Therapeutics (JCET), Krakow, Poland; [2]Jagiellonian University Medical College, Faculty of Medicine, Chair of Pharmacology, Krakow, Poland

Coronary circulation supplies the heart muscle with blood. Promptly, any alteration of coronary vascular homeostasis can contribute to the development of cardiac contractile or relaxation impairment further leading to heart failure. Previous reports by our team have shown that alteration in vascular permeability in large vessels (aorta, brachiocephalic artery, femoral artery) is an early marker of endothelial dysfunction and can occur before functional changes[1]. To probe the changes in vascular permeability, the dynamic of macromolecular contrast agent (e.g. albumin labeled with Gd-based contrast agent) can be used. Another hallmark of early vascular dysfunction is oxidative stress, i.e. results of an imbalance between the generation and detoxification of reactive oxygen species. Oxidant stress is known to play a central role in many types of cardiovascular disease including heart failure. Recently, an approach to indirectly assess oxidant stress in the heart[2] was proposed based on the reduction rate of a stable nitroxide radical, which is assumed to stem from the increase in scavenging enzymes in response to increased oxidant stress.

In the present study, we sought to demonstrate the utility of dynamic contrast-enhanced (DCE) MRI to detect cardiovascular changes in coronary vascular permeability using gadolinium-labeled albumin and oxidant stress using nitroxide radical reduction rate. To obtain a quantitative metric, the concentration of contrast agent in the myocardium and the blood pool was calculated based on the saturation recovery approach. The DCE data were recorded using a custom-modified gradient echo-based sequence. The contrast agent concentration was calculated based on changes in $T_1$ relaxation as described previously[3]. As a model of cardiac dysfunction a translational model of heart failure with preserved ejection fraction was used encompassing a high-fat diet and L-NAME treatment. The results of the DCE analysis of coronary vascular permeability and oxidant stress were compared with standard metrics of cardiac function.

References:
1) DOI: 10.1002/nbm.3567. 2) DOI: 10.1002/nbm.4359. 3) DOI: 10.1016/j.acra.2006.02.040.

**Information on brain tissue microstructure obtained from MRI signal phase**

Harald Moeller

Max Planck Institute for Human Cognitive and Brain Sciences, Leipzig, Germany

Magnetic resonance imaging (MRI) yields information on iron deposits and myelin content in brain tissue *in vivo* on a submillimeter spatial scale. Both compounds are major contributors to the water spin relaxation and magnetic susceptibility. In the context of this presentation, the focus is on information that can be extracted from the MRI signal phase. Briefly, the phase reflects the mean intravoxel magnetic field distribution. This provides a measure of the local susceptibility distribution, which can be related to tissue composition and microstructure.

On a more fundamental level, anisotropic properties of susceptibility were studied in entire fixed chimpanzee brains by reorienting the specimen in the magnetic field. Such data allow to estimate primary axonal trajectories using mono-tensorial models. An integration of additional information from the decay of the signal magnitude in multi-echo acquisitions achieves a separation of contributions from diamagnetic (dominated by myelin) and paramagnetic (dominated by iron content) compounds. Modeling of more complex fiber structures within a voxel, such as intersecting bundles, or an estimation of orientation distribution functions is also possible providing similar information as obtained with high angular resolution diffusion imaging techniques.

## Ensuring data quality, reliability, and reproducibility through Quality Assurance Procedures in Preclinical in (PET)/MR

Francesco Moneta, Claudia Oerther, Tim Wokrina

Bruker BioSpin MRI GmbH, Rudolf-Plank-Straße 23, 76275 Ettlingen, Germany

**Introduction:** Quality Assurance (QA) is process of checking functionalities and the reproducibility of their outcome. Quality depends on several factors such as the method used, the setup, the sample, the workflow and the PET and MRI system condition. QA procedures should be performed at defined time points to monitor system performances and guarantee reliability of results. MRI systems may differ because of configuration and brand, users should verify QA procedure results when comparing data from different systems.

**Methods:** Every Bruker system is delivered with QA protocols and standard phantoms. QA procedures cover image quality: homogeneity, signal to noise ratio (SNR), image ghosting, water suppression, temporal stability and apply to: spin echo (MSME), gradient echo (FLASH), and among the most demanding sequences in terms of eddy current distortions: fast spin echo (RARE), volume selected spectroscopy (PRESS), echo planar imaging (EPI). To properly perform QA loading phantoms are used in combination with phantom holders for reproducible positioning. Phantoms contain a fluid with defined chemical composition that imitates the loading of a certain animal body part. QA tests are automatically performed


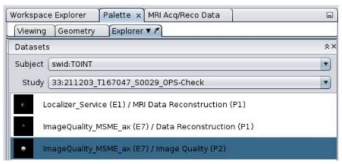


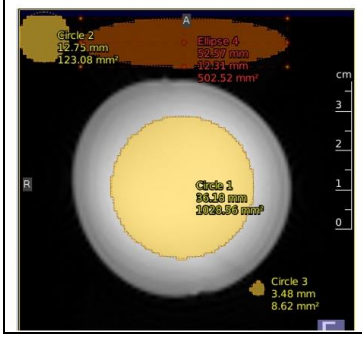


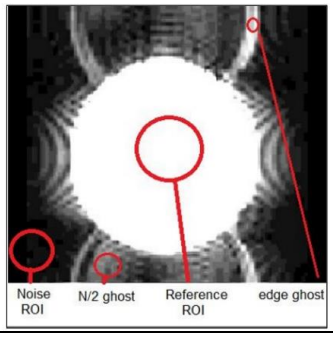


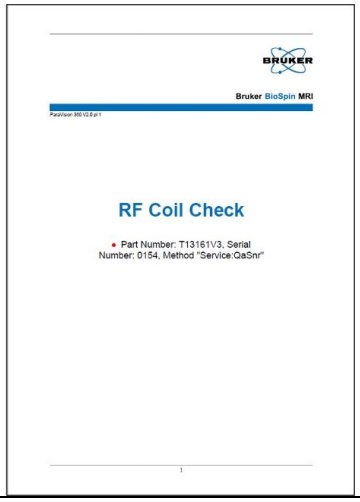

and stored; results saved in a report (Fig.1).
Fig. 1: Phantom and holder positioned under RF-coil. QA MRI methods, Ghost detection algorithm: report of QA procedure.
Results/Discussion:
Analyzing hundreds of QA protocols during installation and maintenance of preclinical MRIs with different configurations (field strength, gradient strength, shim strength, etc. shows that ghost level on FLASH, MSME, RARE is <2.5%, Nyquist N/2 ghost level in EPI is always <5%, and edge ghost level is always <10%. The temporal stability in EPI is <2%. The water linewidth of a 3x3x3 mm3 voxel is <0.05 ppm, the eddy current spectral distortion is < 2.5%, the on-resonance water suppression factor is >500, and 0.7 ppm off-resonant <1.2. Only the SNR results are RF-coil individual. The above specifications must be met also when a PET-insert is used in combination with an MRI. PET/MRIs that do not meet these specifications, often have a problem with eddy current compensation or shim calibration, field drift prevention, can be diagnosed. As a vendor it is important to have a common quality procedure applicable to every configuration in order to verify if the system is in specs.
**Conclusion:** We propose to perform regular QA tests with standardized phantoms to verify the functionality of the instrument and the capability of providing true quantification. An automatic QA test protocol with an automatic quantitative output report is provided as a starting point (QA_SNR). Mapshim calibration, pulse power and ghosting quantification are available on an admin level and can be made available to the scientific community.

**Photon-counting detectors in pre-clinical & m-CT imaging - benefits and challenges**

Martin Pichotka

Medical Center – University of Freiburg, Department of Radiology, Medical Physics Division, AMIR Core Facility, Freiburg, Germany

Following years of relentless efforts by a dedicated scientific community, photon-counting detectors (PCDs) are by now approaching technological maturity. With the first scanners equipped with this technology being operated in clinical routine, benefits in terms of spatial resolution, noise suppression and improved spectral performance over DECT have been widely published in the recent past.
However, due to their technological complexity and particular characteristics, which differ strongly from previous generations of X-ray detectors, PCDs remain a challenge for system developers and methods developers alike, requiring further research to realize the full potential of the technology.
In our presentation, we will address the current state of PCD technology, as well as some remaining challenges. A particular focus will be put on high-resolution X-ray imaging using PCDs. Here fabrication dependent limitations on the pixel size (currently ~50micron) only appear to be the limiting factor.

**Tracking of immune cells using $^{19}$F MR imaging in a murine model of pancreatic cancer under therapy**

Wilfried Reichardt[1], Yayu Li[1], Philipp Hafner[2], Steffen Keller[2], Huda Jumaa[2], Chen Xun[2], Asma Alrawashdeh[2], Dominik von Elverfeldt[1] und Dietrich A. Ruess[2]

[1]Division of Medical Physics, Department of Diagnostic and Interventional Radiology, University Medical Center Freiburg, Faculty of Medicine, University of Freiburg, Freiburg, Germany. [2]Department of General and Visceral Surgery, University Medical Center Freiburg, Faculty of Medicine, University of Freiburg, Freiburg, Germany

$^{19}$F magnetic resonance imaging has emerged as a powerful tool for noninvasive longitudinal imaging of immune cells in vivo [1] in oncologic mouse models [2]. In this study, we investigated the potential of $^{19}$F MRI to monitor the immunomodulatory effects of dual SHP2/MEK inhibition in a genetic mouse model of pancreatic cancer. We used a tumor model, which involves a strong and characteristic inflammatory tumor microenvironment.

Mice were randomly assigned to different treatment groups (n=4x5) when a tumor was detectable. To label the immune cells internally with perfluorocarbon (PFC) emulsion, we injected the formerly commercially available perfluorocarbon emulsion V-Sense DM-Green (Celsense) according to the manufacturer's recommendations 24h before initiation of treatment. MRI experiments were performed on a Bruker 9,4 T Biospec system imaging using two separate mouse volume quadrature-resonators (Bruker, Ettlingen, Germany). MRI was performed at serial time points (24h after injection of the nanoemulsion, 1 week and 2 weeks later). Tumor volumetry showed a decreased volume in all of the treated groups, most prominently in the group treated with the combination therapy. $^{19}$F MRI detected an increased accumulation of labelled immune cells in the tumor in the treated groups, again most pronounced in the group treated with a combination. In addition to tumor volumetry, we could show that it is possible to track immune cells in the KPC genetic mouse model for pancreatic cancer using $^{19}$F MR imaging.

References:
1. Chapelin F, Capitini CM, Ahrens ET. Fluorine-19 MRI for detection and quantification of immune cell therapy for cancer. J Immunother Cancer. 2018 Oct 11;6(1):105. doi: 10.1186/s40425-018-0416-9. PMID: 30305175; PMCID: PMC6180584.
2. Croci D, Santalla Méndez R, Temme S, Soukup K, Fournier N, Zomer A, Colotti R, Wischnewski V, Flögel U, van Heeswijk RB, Joyce JA. Multispectral fluorine-19 MRI enables longitudinal and noninvasive monitoring of tumor-associated macrophages. Sci Transl Med. 2022 Oct 19;14(667).

**Contrasting properties of hybrid nanosilica and cerium oxide nanoparticles for potential theranostic applications**

Natalia Łopuszyńska[1], Kamil Stachurski[1], Terje Didriksen[2], Juan Yang[2], Anna Lind[2], Sacha Muller[2], Magdalena Regulska[3], Monika Leśkiewicz[3], Magdalena Procner[3], Krzysztof Jasiński[1], Władysław Lasoń[3], Piotr Warszyński[4], Władysław P. Węglarz[1]

[1]Institute of Nuclear Physics Polish Academy of Sciences, Cracow, Poland; [2]SINTEF Industry, Department of Process Technology, Oslo, Norway; [3]Maj Institute of Pharmacology Polish Academy of Sciences, Cracow, Poland; [4]Institute of Catalysis and Surface Chemistry Polish Academy of Sciences, Cracow, Poland

The aim of the present study was to evaluate the MRI contrasting properties of a series of new nanoparticles that can be classified into two categories: HNS (Hybrid Nanosilica)-based nanoparticles (NPs): HNS, HNS-Gd, lactamide-HNS-Gd, $^{19}$F-HNS and ceria-based NPs: $CeO_2$ and $CeO_2$-Gd. While the ceria nanoparticles have already been investigated for their neuroprotective effect, HNS can be easily further functionalized for theranostic purposes.

For the Gd-based nanoparticles, contrasting properties were investigated by the measurement of molar relaxivities $r_1$ and $r_2$ and by the contrast assessment in $T_1$- and $T_2$-weighted images. The specific molar relaxivities $r_1$ results of HNS NPs were as follows: 2.12 $mM^{-1}s^{-1}$ (HNS-Gd in PBS), 0.0012 $mM^{-1}s^{-1}$ (HNS in PBS), 2.49 $mM^{-1}s^{-1}$ (Lactamide HNS-Gd), and 1.88 $mM^{-1}s^{-1}$ (HNS-Gd in water). Interestingly**,** HNS-Gd in PBS exhibited a relatively high $r_2$ value of 105.03 $mM^{-1}s^{-1}$, which can be attributed to binding to PBS particles and the creation of large molecules. Such a nanoparticle solution showed strong cytotoxic properties, while a similar effect was not observed for HNS-Gd in water. Modification of HNS-Gd with lactamide suppressed the $T_2$ effect ($r_2$ = 6.77 $mM^{-1}s^{-1}$ for lactamide-HNS-Gd) and significantly lowered cytotoxicity. Regarding $CeO_2$-based nanoparticles, MR relaxation results showed that the contrasting properties of $CeO_2$-Gd nanoparticles arise almost entirely from the presence of Gd ($r_1$ = 0.75 $mM^{-1}s^{-1}$ for $CeO_2$). $CeO_2$-Gd nanoparticles have excellent positive contrasting properties, as described by the very high $r_1$ value of 32 $mM^{-1}s^{-1}$, which was also greatly visible in MR images. $CeO_2$-Gd were non-toxic in the whole analyzed concentration range. Moreover, in the experiment with 0.5 mM $H_2O_2$, $CeO_2$-Gd nanoparticles exhibited a neuroprotective effect.

$^{19}$F-HNS exhibits preferable characteristics for $^{19}$F MRI, i.e. it has a $^{19}$F NMR spectrum with a single peak and relatively short $T_1$ relaxation time of 2.5 s and long $T_2$ time of 1.8 s. $^{19}$F

imaging was accomplished with a standard FLASH imaging sequence in a reasonable timeframe of 30 min. The SNR was around 15, which suggests that this time could be shortened, or spatial resolution increased. Moreover, $^{19}$F-HNS was non-toxic in the whole concentration range, making the proposed NPs a good candidate for further in-vivo investigations.

Acknowledgements:
This work was supported by the National Centre of Science (NCN) of Poland, grant nr: 2019/34/H/ST5/00578 (GRIEG-1, funded under the Norwegian Financial Mechanism).

**Metabolic MRI: is it useful or confusing?**

Greg Stanisz

Sunnybrook Research Institute, University of Toronto, Toronto, Canada.
Canada Research Chair in Cancer Imaging, Tier I

The role of non-invasive imaging in managing cancer patients has increased beyond localization of solid tumour pathology and it now encompasses image-guided therapy, monitoring treatment and identification of the tumour grade, allowing for more precise and effective management of cancer patients. Currently, in the standard of care, response assessment is performed by evaluating changes in linear tumour dimensions; however, it may take weeks to months before significant changes occur, by which time the therapeutic window is often lost. Assessing tumour response early after the treatment enables to identify responders from non-responders and may allow for a change of treatment.

We suggest that saturation transfer MRI (ST-MR), a novel MRI technique, permits the robust evaluation of tumour micro-environment including regions with high metabolic activity and is capable of detecting early cell death (apoptosis) following treatment. We have recently applied these techniques in patients with brain metastasis undergoing stereotactic radiosurgery (SRS) and glioblastoma multiforme (GBM). To date, we have scanned ~500 patients with High Grade Glioma (HGG) and brain metastases (BM).

1. In HGG, we observed that ST-MRI can identify which patients will progress as early as two weeks into their 6-week treatment.
2. Changes in tumour metabolism (CEST) allow for separation of responders from nonresponders one week post-treatment of BM. qMRI can predict the amount of tumour shrinkage in BM at least one month before treatment.
3. CEST allows the assessment of treatment-induced side-effects of radiation treatment and permits distinguishing between tumour progression and radiation-induced necrosis.
4. Even before treatment begins, several ST metrics can assess tumour aggressiveness and predict patient response.

We have also demonstrated great potential in assessing tumour and NAWM environment in Low-Grade Gliomas and its ability to predict further damage.

Similar techniques could be also used in detecting metabolic changes in the brain as a result of neurological disorders. ST-MRI has been successfully used in probing glucose metabolism in Alzheimer's Disease and in modulation of GABA/Glutamate cycle in animal models of anxiety disorders using probiotics. It may be also possible to probe metabolites associated with serotonin pathway non-invasively.

In summary, metabolic MRI (such as ST-MRI) may serve as a non-invasive tool to monitor the effects of treatment for various disorders.

**In vivo Potassium MR-Spectroscopy at 7 T. Establishment and first Applications in Human Muscle**

Peter Vermathen

MR Methods, DIN & DBMR, University & Inselspital Bern, Switzerland

Potassium and sodium play vital roles in numerous cellular processes. Low potassium intake associates with cardiovascular disease and mortality, while beneficial effects of higher potassium intake have been demonstrated. Since serum or urine potassium levels

correlate poorly with tissue potassium, its specific determination in different organs would be very valuable. Existing methods are invasive, associated with radiation exposure and lack spatial resolution.

In vivo determination of 39K was not possible until very recently. By using 39K MRI and MR spectroscopic imaging (MRSI) at ultrahigh magnetic fields for the first time a non-invasive and spatially resolved method for in vivo investigation of the important K+ ion homeostasis and of normal cell membrane function i.e., Na+-K+-ATPase function in humans has become feasible which has recently been convincingly demonstrated [1,2].

Here we present our implementation and initial results on using 39K MR spectroscopy. Initial applications include the spatially resolved measurement of quadrupolar splittings in human calf muscles based on previous studies [1,3] using a modified CSI-FID sequence. This may prove valuable for 39K quantification in MRSI investigations. Furthermore, an initial exercise study within the magnet was performed, suggesting fast potassium decrease during exercise followed by fast recovery afterwards.

References:
1. Gast LV, Völker S, Utzschneider M, Linz P, Wilferth T, Müller M, et al. Combined imaging of potassium and sodium in human skeletal muscle tissue at 7T. Magn Reson. Med 2021;85:239.
2. Umathum R, Rösler MB, Nagel AM. Radiology, 2013, 269, 569.
3. Rösler MB, Nagel AM, Umathum R, Bachert P, Benkhedah N. NMR in Biomed. 2016, 29: 451.

## $T_1$ determination with rapid 2D Gradient Echo Imaging also applicable in cardiac MRI

Astrid Wietelmann[1], Clemens Müller[2], Arno Nauerth[3], Thomas Braun[4]

[1]Max-Planck-Institute for Heart and Lung Research, Bad Nauheim, Germany; [2]Kerckhoff-Klinik, Bad Nauheim, Germany; [3]IntraGators.com, Germany; [4]Max-Planck-Institute for Heart and Lung Research, Department I Cardiac Development and Remodelling, Bad Nauheim, Germany

**Introduction:** Cardiac mouse MRI is a widely used method to study and characterize intrinsic tissue structure and physiology with e.g. determination of $T_1$ and $T_2$ relaxation time constants, diffusion coefficients or kinetic parameters of contrast agent uptake in cardiovascular diseases [1]. As exact $T_1$ values are so far only derived from time-consuming 3D experiments [2], we want to present a tool to calculate images with quantitative $T_1$ values out of a flip angle varied 2D gradient echo experiment like FLASH or IntraGateTM under the consideration of the excitation pulse profile of the slice selection pulse.

**Methods:** Measurements were performed on a 7T (PharmaScan, cryogenic 4 element array receive-only or 30mm $^1$H planar receive-only surface coil, 72mm transmit-only volume coil, Bruker Biospin) small animal MRI system. Utilizing 2D gradient echo sequences and the T1Gator Tool (Arno Nauerth; https://IntraGators.com), we achieved images with quantitative $T_1$ values for CuSO4 x 2H2O phantoms with and without gadobenate dimeglumine (Gd-
BOPTA, MultiHance™).

**Results/Discussions:** Our T1Gator Tool enables us to calculate $T_1$ values for 2D Gradient Echo type of experiments: The signal of a 3D experiment depends on the applied flip angle and the TR. In 2D, the RF profile correction of the applied slice selection pulse has to be taken into account (RfProfileGator Tool, A. Nauerth: https://IntraGators.com). Exemplary the expected signals of a $T_1$ of 400ms (green) and 1000ms (blue), at TR of 10ms and flip angles from 0 to 90 degrees are shown in Fig.1. The highest dynamic corresponds to low flip angles.

$T_1$ calculation of a sample with a $T_1$ of about 100ms, acquired with the flip angles 1.5, 8, 11, 18 and 25 degrees at a TR of 10ms is shown in Fig. 2 and Fig. 3, the graphs on the right show the measured values in black and the theoretical ones in blue. Fig. 3. Fig. 4 shows the profile of the applied excitation pulse.

**Conclusion:** We have successfully established a quantitative $T_1$ determination for 2D Gradient Echo types of experiments.

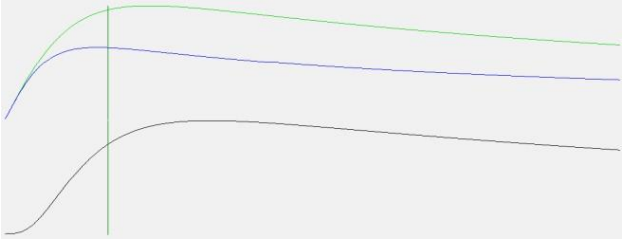

Fig. 1: Expected signal for two different $T_1$ values.
Black curve indicates the difference between the two expected signals at 400 ms and 1000 ms.

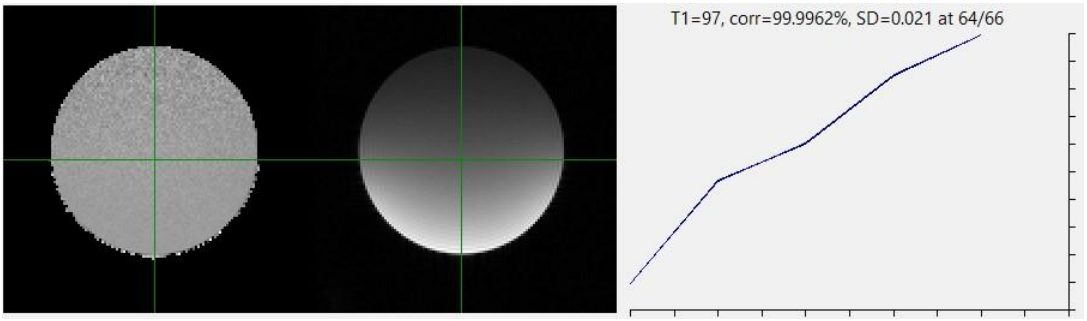


Fig. 2: $T_1$ calculation. Left image shows the calculated $T_1$ image, the right one is the image taken at a flip angle of 8 degree, at the crossing of the green lines a $T_1$ of 97 ms was calculated with a correlation of 99.996% of the theoretical value with a standard deviation of 0.021ms.

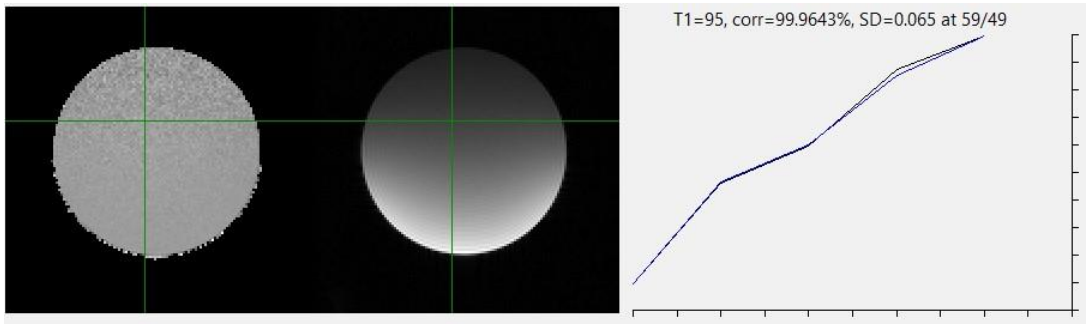


Fig. 3: Visualization of the deviation between measured (black) and theoretical (blue) values.

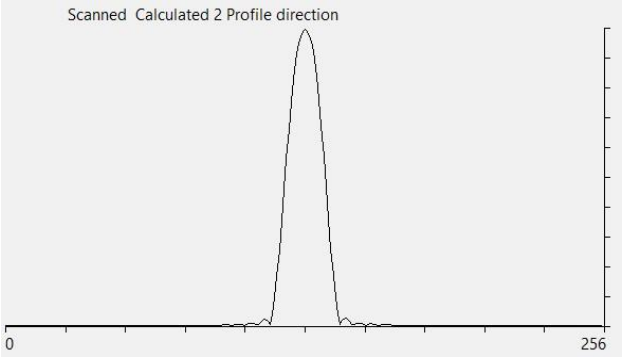


Fig. 4: Visualization of the calculated excitation pulse profile.

References:
1. Wu YL "2021: "Cardiac MRI Assessment of Mouse Myocardial Infarction and Regeneration" Methods Mol Biol 2158:81-106.
2. Coolen BF, et al. (2011) "Three-dimensional $T_1$ mapping of the mouse heart using variable flip angle steady-state MR imaging" NMR Biomed. 24(2):154-62.

**In vivo monitoring of gut inflammation in the insect larvae of *Manduca sexta* by $^{19}$F magnetic resonance imaging**

Anton G. Windfelder

Fraunhofer IME , Department Bioresources, Giessen, Germany; Justus Liebig University Giessen,

Clinic for Diagnostic and Interventional Radiology, Giessen, Germany

Mammalian model organisms are increasingly subjected to ethical concerns and restrictions (3R Principle). Therefore, we have established the insect larva of *Manduca sexta* as a new alternative model organism for the $^{19}$F-based detection of inflammation in magnetic resonance imaging.

We used bacteria-induced gut inflammation as a positive control to demonstrate the feasibility of $^{19}$F-MRI in insects using nanoemulsions of perfluorocarbons (PFCs) at 9.4 T. Simultaneous acquisition of morphologically matching fluorine ($^{19}$F) and proton ($^{1}$H) images enabled an anatomic localization of PFCs after application in the anterior and posterior midgut region of the insect larvae. Afterward, an ex vivo examination of the insect's midguts confirmed inflammatory lesions in the anterior and posterior midgut regions with severe melanizations. In independent experiments using flow cytometry and rhodamine-labeled PFCs, we determined plasmatocytes and granulocytes, the two main fractions of *Manduca sexta* hemocytes ("White Blood cells" of insects), as a sink for injected PFC nanoparticles. Further, plasmatocytes and granulocytes showed significant percentual alteration from non-inflamed control animals, confirming the positive control's inflammatory status.

Since innate immunity is highly conserved between insects and mammals, insect larvae are suitable as alternative 3R-compatible in vivo animal models for screening new contrast agents, protocols, and imaging modalities. Also, this imaging platform may allow the sublethal detection of insect inflammation as a persuasive new tool in ecotoxicology.

## Synthesis and characterization of multifunctional nanoparticles for potential theranostic applications

Juan Yang[1]

[1]SINTEF Industry, Department of Process Technology, Oslo, Norway;

## The application of $^{19}$F NMR spectroscopy in biomolecular studies as a potent technique for structural analysis of the proteins and protein-protein complexes in solution

Lesia Kolomiiets, Igor Zhukov

Laboratory of Biological NMR, Institute of Biochemistry and Biophysics, Polish Academy of Sciences, Warsaw, Poland

The application of $^{19}$F NMR spectroscopy in structural studies of proteins has emerged as a potent tool within the other methods of structural biology. While the classical spectroscopic methods, such as $^{1}$H, $^{13}$C, and $^{15}$N NMR, routinely used to structural analysis proteins in solution, the utilization of $^{19}$F NMR gains a couple of new possibilities to contribute in structural studies. Specifically, the 100% naturally abundant of the $^{19}$F nucleus, makes it an ideal candidate for NMR analysis. With a spin of 1/2 and a high gyromagnetic ratio, $^{19}$F isotope exhibits exceptional sensitivity, approximately 83% that of $^{1}$H. The shielding of the $^{19}$F nucleus is predominantly governed by a substantial chemical shift anisotropy (CSA). Consequently, fluorine chemical shifts are exquisitely responsive to variations in the local molecular environment, boasting a chemical shift range nearly 100 times larger than that of $^{1}$H. Another advantage of employing $^{19}$F as an NMR probe lies in its virtual absence from the majority of naturally occurring biomolecules. This characteristic allows for the investigation of fluorinated proteins in a wide range of routinely used buffer systems and environments, without interference from background signals. Furthermore, the van der Waals radius of the $^{19}$F atom, measuring 1.47 Å, positions it between the VdW radii of hydrogen (1.2 Å) and oxygen (1.52 Å) suggesting that incorporating $^{19}$F instead of $^{1}$H nuclei has minimal perturbing effects and often exerts little influence on a protein's biological activity.

In the Laboratory of Biological NMR, we perform the synthesis and purification of the

protein, containing fluorinated versions of aromatic residues - tryptophan, phenylalanine, and tyrosine. Based on these achievements, we performed several research projects focused on the structural analysis of the proteins and protein-protein complexes utilizing $^{19}F$ NMR spectroscopy. Our recent experimental findings affirm that the incorporation of fluorine atoms into aromatic residues makes it possible to obtain valuable experimental data about localization structural modifications, ligand binding, conformational dynamics, and protein interactions at the atomic scale. At the moment, the $^{19}F$ NMR spectroscopy seems to be a promising and cost-effective technique, which substantially increases our knowledge about complex biomolecular systems.

# Short Oral Presentations

**Correlative multimodal biomarker identification of three breast cancer molecular subtypes: From image acquisition to machine-learning-based radiomics**

Silvester J. Bartsch[1], Klára Brožová[2,3], Joachim Friske[1], Christoph Fürböck[4], Lukas Kenner[3,5], Klaus Kratochwill[2], Daniela Laimer-Gruber[1], Georg Langs[4], Thomas H. Helbich[1], Katja Pinker[1,6], Thomas Wanek[1]

[1]Division of Structural and Molecular Preclinical Imaging (PIL), Department of Biomedical Imaging and Image-Guided Therapy, Medical University of Vienna, Vienna, Austria; [2]Core Facility Proteomics, Medical University of Vienna, Vienna, Austria; [3]Department of Experimental Pathology and Laboratory Animal Pathology, Medical University of Vienna, Vienna, Austria; [4]Computational Imaging Research Lab, Department of Biomedical Imaging and Image-guided Therapy, Medical University of Vienna, Vienna, Austria; [5]Unit of Laboratory Animal Pathology, University of Veterinary Medicine, Vienna, Austria, [6]Breast Imaging Service, Department of Radiology, Memorial Sloan Kettering Cancer Center, New York, NY, USA

In preclinical research, the availability of capable hybrid imaging systems, such as PET/MRI scanners, as well as readily accessible whole-tumor samples for histological and proteomic analyses, have given rise to correlative multimodal imaging (CMI). CMI enables the cross-validation of in-vivo and ex-vivo imaging biomarkers to get a holistic view on complex processes, such as breast cancer progression. However, the use of CMI for imaging biomarker identification depends on the availability of reproducible data-handling protocols to validate newly investigated biomarkers.

In our project, we developed two CMI protocols for the assessment of metabolic reprogramming and hypoxia-induced neoangiogenesis, two main hallmarks of breast cancer progression. Our aim is to provide a guideline for the acquisition of PET/MRI, fluorescent multiplex immunohistochemistry (mpIHC), and MALDI mass spectrometric imaging (M-MSI) datasets for a machine-learning based identification of imaging biomarkers in luminal A, Her2+ and triple-negative breast cancer molecular subtypes.

Xenograft models of three breast cancer molecular subtypes were measured using simultaneous [$^{18}$F]-FDG PET/glucoCEST MRI or a combination of [$^{18}$F]-FMISO PET with diffusion-weighted, blood-oxygen-level dependent and contrast-enhanced MRI. Following in-vivo imaging, tumors were resected and prepared for mpIHC and M-MSI. Data from in-vivo and ex-vivo imaging were resampled, normalized and co-registered for machine-learning-based biomarker identification.

We conclude that our protocols provide a suitable guideline for the rapid and reproducible acquisition of CMI datasets. These protocols will enable the identification of in-vivo PET/MRI imaging biomarkers, validated by ex-vivo mpIHC and M-MSI, paving the way for holistic imaging of metabolic reprogramming and hypoxia-induced angiogenesis in the investigated breast cancer molecular subtypes.

**Design of Smart Nanoprobes for $^{19}$F-MRI Detection of MMP-2/9 in Stroke**

Karen Contreras-Muñoz[1,2], Mónica Carril[1,2,3]

[1]Instituto Biofisika (CSIC, UPV/EHU), Leioa, Bizkaia, Spain; [2]Departamento de Bioquímica y Biología Molecular, UPV/EHU, Leioa, Bizkaia, Spain; [3]Ikerbasque, Basque Foundation for Science, Bilbao, Spain

Ischemic stroke is one of the main cerebrovascular diseases responsible for thousands of deaths across the EU. It has been shown that matrix metalloproteinases (MMPs) 2 and 9, which are gelatinases, perform important roles in blood-brain barrier disruption during ischemic stroke, but there is no specific probe for imaging and recognizing them [1]. Thus, there is a need for the development of specific diagnostic and therapeutic strategies targeting MMP-2/-9. We propose the design of a smart fluorinated probe encapsulated in gelatin as an ON/OFF contrast agent for $^{19}$F-MRI for the detection of MMP-2/-9 (Figure 1A). The OFF state would be achieved by the encapsulation of a fluorinated probe, and such probe release through gelatin digestion by MMP-2/9 would lead to the ON state.

Preliminary unpublished results by our group showed that it is possible to both encapsulate highly fluorinated nanoparticles of small gold core (F-Au-NPs) [2] in gelatin carriers and to quench the $^{19}F$ signal (Figure 1B-C). Gelatin NPs are synthetized via a two-step desolvation method with acetone and EDC/NHS as crosslinking agents. F-Au-NPs are prepared with fluorinated PEG ligands by the reduction of $HAuCl_4$ with $NaBH_4$. The so obtained NPs are then conjugated to gelatin chains and further encapsulated into gelatin nanospheres following a similar procedure as with gelatin NPs synthesis. The procedure is being optimized to improve fluorine loading and gelatin NPs solubility.

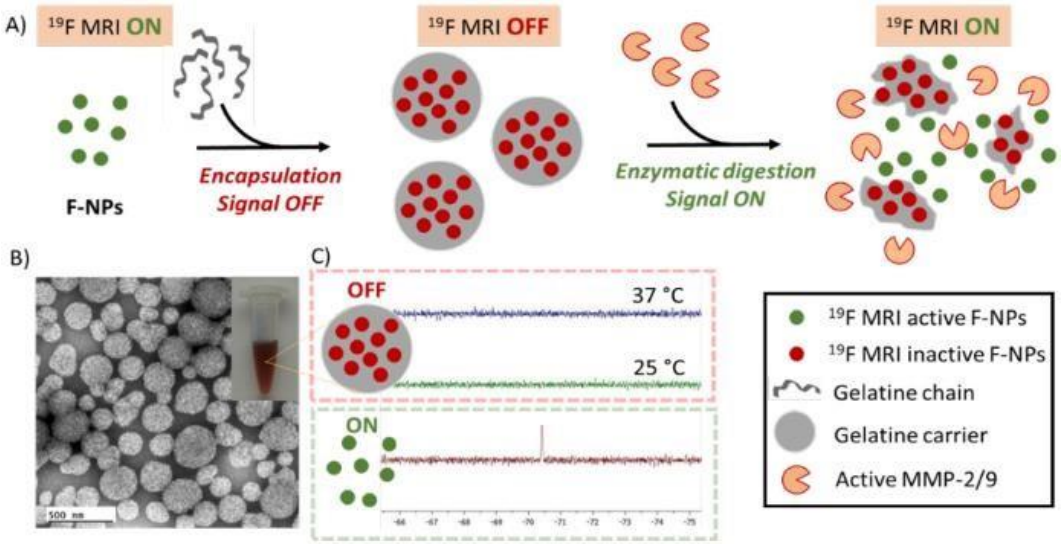


Image 1 A) General performance of the ON/OF contrast agent. B) Negative staining TEM micrograph showing gelatine Au F NPs. C) 19 F NMR spectra showing the expected signal from a F NP solution (ON) and the quenched signal of F NPs encapsulated in gelatine (OFF).

References:

1. Zinnhardt, B. et al., Multimodal imaging reveals temporal and spatial microglia and matrix metalloproteinase activity after experimental stroke. J. Cereb. Blood Flow Metab. 2015, 35, 1711-1721.

2. Arango, J. M. et al., Fluorine labeling of nanoparticles and in vivo $^{19}F$ Magnetic Resonance Imaging. ACS Appl. Mater. Interfaces 2021, 13, 12941-12949.

**Biocompatible Polymer for Real-Time ROS-triggered changes in $^{31}$P-MR and optical imaging**

Natalia Jirát-Ziółkowska[1,2], Kateřina Sulková[1], Lucie Kracíková[3,4], Ladislav Androvič[3], Dominik Havliček[1,2], Richard Laga[3], and Daniel Jirák[1]

[1]Institute for Clinical and Experimental Medicine, Prague, Czech Republic; [2]Institute of Biophysics and Informatics, First Faculty of Medicine, Charles University, Prague, Czech Republic; [3]Institute of Macromolecular Chemistry, Czech Academy of Sciences, Prague, Czech Republic; [4]Faculty of Chemical Technology, University of Chemistry and Technology, Prague, Czech Republic

Hydrophilic polymers have emerged as versatile tools for X-nuclei magnetic resonance (MR) [1 – 4]. This study introduces biocompatible probes consisting of hydrophilic phosphor- and fluoropolymers for $^{31}P/^{19}F$-MR. Additional responsiveness to physiological conditions enables real-time functional imaging of the body to localize pathologies and assess Reactive Oxygen Species (ROS) generated in these conditions. The $^{31}$P-MR challenges associated with strong biological phosphorous background signals were solved by the biologically rare phosphorothioate (P=S) group incorporated into the polymer structure. In the presence of ROS, the P=S group undergoes oxidation to phosphoester group P=O (δ=0 ppm), triggering a detectable chemical shift (δ=60 ppm) in $^{31}$P-MRS under different oxidative conditions ($H_2O_2$, NaClO and cancer cell lines). ROS production was

confirmed by fluorescent experiments with a 4T1 cell line, derived from mouse breast cancer, where the conversion of OxyBurst dye (OB) to its fluorescent derivative was higher in total fluorescence emission ratio compared to the controls (OB in medium alone and with 50 nM-100 nM $H_2O_2$). The $^{31}$P-MRS signal from the P=S group was detected under all tested conditions, including short-time measurements with the significant oxidation-triggered chemical shift in the presence of $H_2O_2$ and NaClO within first hour. Furthermore, there were ROS-triggered oxidation variabilities between cell lines, ranging between 8–14% within 12h. In the *in vivo* experiments, we measured the biodistribution of the probe (retro-orbital polymer injection) and ROS detection (intratumoral polymer injections) under pathological conditions in Balb/C mice tumor model. Additional trifluoromethyl group ($CF_3$) added into the polymer structure for *in vivo* measurements enables precise localization using "hotspot" $^{19}$F-MRI. This metal-free, nontoxic, ROS-responsive probe was rigorously tested *in vitro* and *in vivo* on a 4.7T scanner. The high specificity and responsiveness of the polymer probe render it a sensitive sensor of pathological conditions.

Acknowledgements:
The project was supported by the Ministry of Health of the Czech Republic [NU20-08-00095]; by MH CR-DRO (Institute for Clinical and Experimental Medicine IKEM, IN00023001), and the National Institute for Research of Metabolic and Cardiovascular Diseases (Programme EXCELES, Project no. LX22NPO5104), which is funded by the European Union's Next Generation EU program.

References:
1. D. Jirak, A. Galisova, K. Kolouchova, D. Babuka, M. Hruby, Magn Reson Mater Phy 2019, 32, 173.
2. N. Ziółkowska, M. Vít, R. Laga, D. Jirák, Sci. Rep. 2022, 12, 2118.
3. L. Kracíková, N. Ziółkowska, L. Androvič, I. Klimánková, D. Červený, M. Vít, P. Pompach, R. Konefał, O. Janoušková, M. Hruby, D. Jirák, R. Laga, Macromol. Biosci. 2022, 22, 2100523.
4. T. Rheinberger, U. Flögel, O. Koshkina, F.R. Wurm, Commun Chem. 2023 Sep 1;6(1):182.

**Evaluation of Intra Voxel Incoherent Motion (IVIM) methodology in the context of perfusion clinical protocols**

Kamil Lipiński, Piotr Bogorodzki

Faculty of Electronics and Information Technology, Warsaw University of Technology, Warsaw, Poland

Intravoxel Incoherent Motion (IVIM) is a specific Diffusion-Weighted Imaging (DWI) method in Magnetic Resonance Imaging (MRI). This concept has been proposed to estimate tissue perfusion, as blood flow is similar to a pseudo-diffusion of water molecules. Despite the popularity of DWI in clinical routine, for example in acute stroke phase, application of IVIM however is still uncommon.[1]

The aim of this study was to evaluate robustness of IVIM parameters estimates: f (blood fraction) and D* ("quick" diffusion), across different Signal to Noise Ratio (SNR) levels. As a part of this work, we also developed a toolbox for IVIM-MRI parameters estimation using three basic methods: trust-region single-step fitting, segmented trust-region fitting, and segmented grid search. The toolbox also includes tools for visualization and synthetic signal generation. We implemented this application in the MATLAB environment using AppDesigner for a userfriendly Graphical User Interface (GUI) and Curve Fitting Tool functionalities for the fitting algorithm[2].

Evaluation was conducted on a set of synthetic IVIM data which consisted of 10,000 realizations for each SNR level and was prepared using a constant set of S0 (1000 a.u.), f (0.08), D (0.001 mm/s$^2$) and D$^*$ (0.01 mm/s$^2$) parameters. Each realization included signal generated for the same predefined b-values and was subjected to Rician noise to achieve the desired SNR level calculated as μ/σ, ranging from 15 to 50. Relatively low number of b-values (maximum of 17) was assumed in scanning protocol due to limited scanning time required in clinical practice. Subsequent analysis aimed to demonstrate the estimation error for various blood fractions within a voxel.

The above-mentioned tests shown IVIM to be notably error-prone in "quick" diffusion, particularly in D* parameter where reached levels several hundred percent higher than the

original value. Blood fraction parameter estimation has proven to be more reliable, with values consistently below 50%, when the signal-to-noise ratio (SNR) exceeded 40. This information should be taken in consideration when planning clinical experiments.

References:
1. Le Bihan, D. What can we see with IVIM MRI? *NeuroImage* **187**, 56–67 (2019).
2. The MathWorks Inc. MATLAB version: R2023a. (2023).

## Perfluorocarbon-PLGA particle ultrastructure affects pH sensitivity in $^{19}$F NMR and MRI

Alvja Mali[1,2], Paul B. White[3], Nicolas Stumpe[4], N. Koen van Riessen[1], Cyril Cadiou[5], Françoise Chuburu[5], Mangala Srinivas[1, 6]

[1]Department of Cell Biology and Immunology, Wageningen University and Research, Wageningen, The Netherlands; [2]Leiden University Medical Center, Leiden, The Netherlands; [3]Institute for Molecules and Materials, Radboud University, Nijmegen, The Netherlands; [4]Institute for Molecular Cardiology, Heinrich Heine University, Düsseldorf, Germany (N.S., T.G.-S., U.F.); [5]ICMR Equipe Chimie de Coordination, Universite de Reims; [6]Cenya Imaging B.V., Amsterdam, The Netherlands

Fluorine-19 ($^{19}$F) magnetic resonance imaging (MRI) holds significant promise for quantitative cell tracking. This study explores the relaxation properties of perfluorocarbon (PFC)-loaded nanoparticles (NPs) when coloaded with a paramagnetic Gd chelate (Fig 1).


Fig 1. Schematic of nanoparticles used in this study, including the chemical structure of the gadolinium agents.

Paramagnetic relaxation enhancement (PRE) acts over short distances, necessitating close proximity between the paramagnetic chelate and the nucleus. We investigated whether the internal structure, comparing core-shell and multi-core NPs[1], played a role in the PRE effect of gadolinium (Gd) on the $^{19}$F nuclei. Our initial results underscore the internal structural influence on $^{19}$F MR relaxation. In fractal multi-core NPs, Gd chelate impacts both longitudinal ($T_1$) and transverse ($T_2$) relaxation times, while core-shell NPs mainly exhibit $T_2$ changes. Furthermore, Gd entrapped within the multi-core NPs uniquely enhances $^{1}$H signals in MRI, benefiting from their higher water permeability compared to core-shell NPs [2]. Unexpectedly, multi-core NPs exhibit pH-sensitive transverse relaxation while maintaining stability, unlike core-shell NPs, emphasizing the value of the multi-core structure for $^{19}$F signal enhancement. The pH sensitivity was demonstrated through both $^{19}$F NMR (400 MHz) and MRI (14.1T). The $^{19}$F MRI results clearly illustrate a progressive signal increase from pH 7 to acidic conditions, resembling an “on-off probe”. Additionally, the variation in $T_2$ was confirmed through an in-cell $^{19}$F NMR experiment, revealing changes in $T_2$ values inside and outside the cells, potentially attributable to the acidic environment of the lysosomes.

References:
1. Koshkina O, Lajoinie G, Baldelli Bombelli F, Swider E, Cruz LJ, White PB, Schweins R, Dolen Y, Van Dinther EAW, Van Riessen NK et al: Multicore Liquid Perfluorocarbon-Loaded Multimodal Nanoparticles for Stable Ultrasound and$^{19}$F MRI Applied to In Vivo Cell Tracking. Advanced Functional Materials 2019, 29(19):1806485.
2. Internal Structure of Gadolinium and perfluorocarbon-loaded polymer nanoparticles affects $^{19}$F MRI relaxation times.Nanoscale, 2023, DOI: 10.1039/D3NR04577C.

## DTI reveals age-related changes in brain gray matter in healthy young to middle-aged adults

Zofia Schneider[1], Agnieszka Słowik[2], Artur T. Krzyżak[1]

[1]Faculty of Geology, Geophysics, and Environmental Protection,' AGH University of Krakow, Krakow, Poland; [2]Neurology Clinical Department, University Hospital, Krakow, Poland

**Introduction:** The aging process induces significant morphological changes in the brain, which can be quantified using non-invasive diffusion tensor imaging (DTI) that offers valuable insights into tissue structure and integrity. While previous studies primarily focused on white matter (WM), revealing substantial age-related changes of DT metrics of its pathways [1], the influence of age on gray matter (GM) diffusion properties remain understudied, despite known age-related GM volume reduction [2]. This study aims to investigate associations between age and DT metrics in a wide range of brain structures among young and middle-aged healthy adults.

**Methods:** The study involved 80 healthy individuals (55 females and 25 males), aged from 21 to 50 years (mean age ± standard deviation: 34.3 ± 8.2). Brain MRI for all study participants were acquired using a 3T Siemens Magnetom scanner in the University Hospital in Krakow, Poland. The imaging protocol included a $T_1$-weighted MPRAGE sequence and a spin-echo echo-planar imaging (EPI) sequence with 20 directions of diffusion gradients; b factor of 0, 1000 and 2000 s/mm2; TR, 3900 ms; TE, 88 ms; voxel size, 2.5 x 2.5 x 2.5 $mm^3$; field of view, 191 x 191 $mm^2$; number of slices, 50. For each brain segmentation of 95 anatomical structures was generated using the Fast Surfer (FS) software [3]. The DT was calculated using the b-matrices obtained using BSD, a method for reducing systematic errors [4]. The analysis included 21 DTI parameters, comprising fractional anisotropy (FA), axial (AD), radial (RD), and mean diffusivity (MD), DT elements, eigenvalues and invariants, ultimate anisotropy indices and lattice index [5].

**Results:** For every examined DT parameter, there was a statistically significant correlation with age in at least one ROI. The structure most sensitive to age was the cerebral cortex both as a whole and its individual parts, such as posteriorcingulate, precentral and postcentral where the Pearson correlation coefficient *r* between age and some DT metrics (e.g. MD and AD) was above 0.5. In other structures composed of GM, such as the right thalamus, caudate, putamen or cerebellar cortex, changes in certain parameters with age have also been found. Regarding the cerebral white matter, there were no changes in FA with age, only relatively weak correlations (*r* between -0.3 and -0.2) with several parameters describing the intensity of diffusion. In contrast, stronger correlations for a wider range of parameters were discovered in the cerebellar white matter.

**Conclusion:** Our study showed that significant age-related changes in brain tissues are discernible even in relatively young healthy adults. Furthermore, the results suggest that changes in GM structure and integrity manifest earlier compared to those in cerebral WM. The associations found may improve our understanding of neurodegeneration and age-related processes in the central nervous system.

**Acknowledgements:**
The work was financed by Medical Research Agency contract no: 2020/ABM/01/00006-00.

**References:**
1. Cox S. et al. Nat. Commun. (2016). 2. Narvacan K et al. Hum Brain Mapp. (2017).
3. Henschel L. et al. NeuroImage (2020). 4. Krzyżak A. et al. Magn. Reson. Imag. (2015).
5. Kingsley P. Concepts in Magnetic Resonance Part A (2006).

## $^{19}$F Magnetic Resonance Imaging in Experimental Subarachnoid Hemorrhage

Felix Schoknecht[1], Katharina Tielking[1], Pia Pötschner[1], Shuheng Liu[1], Melina NieminenKelhä[1], Susanne Mueller[2], Stefan P Koch[2], Philipp Boehm-Sturm[2], Peter Vajkoczy[1], Ran Xu[1]

[1]Department of Neurosurgery, Charité - Universitätsmedizin Berlin, corporate member of Freie Universität Berlin, and Humboldt-Universität zu Berlin, and Berlin Institute of Health.
[2]Department of Experimental Neurology, Charité - Universitätsmedizin Berlin, corporate member of Freie Universität Berlin, Humboldt-Universität zu Berlin, and Berlin Institute of Health.

**Background:** Subarachnoid hemorrhage (SAH) caused by rupture of an intracranial aneurysm leads to bleeding in the subarachnoid space (SAS). Secondary brain injury and

associated inflammatory events following SAH originate from extravasated blood and immune cells. Previous evidence has shown that nanoemulsions prepared from perfluoro-5-crown-15-ether (PFCE) preferably label inflammatory cells, clearing the nanoparticles from circulation by phagocytosis. The advantageous lack of $^{19}F$ background enables specific *in vivo* detection of inflammatory foci by $^{19}F$ MRI via immunocompetent PFCE-loaded cells. Thus, we aimed to visualize immune cell and erythrocyte clearance, as well as clot lysis after SAH using PFCE.

**Methods:** A filament perforation surgery was performed to induce SAH in C57BL/6 mice, and Sham operation was done for the corresponding control group. Following the surgery, mice received an intravenous injection of the PFCE nanoemulsion. Accumulation of $^{19}F$ particles was visualized at different time points *in vivo* by $^{1}H/^{19}F$ 7T MRI and evaluated by volume of interestbased approaches and incidence maps. Immunofluorescence staining for nuclei, arachnoid cells, microglia, macrophages, and neutrophils was analyzed by confocal imaging to elucidate the histological location of rhodamine labeled PFCEs. Isolation and characterization of subpopulations of $^{19}F$ particle phagocyting immune cells were performed using flow cytometry.

**Results:** $^{1}H/^{19}F$ MRI revealed an accumulation of PFCEs in the ipsilateral SAS and adjacent brain parenchyma following SAH. Group differences regarding leptomeningeal infiltration of PFCEs into the superior parts of the SAS were observed. Confocal imaging verified the accumulation of PFCEs in the above-mentioned areas, and showed colocalization and spatial affinity to microglia, macrophages, and neutrophils after SAH.

**Conclusion:** PFCE nanoemulsions generate positive $^{19}F$ MRI contrast for visualization of immune cell and blood accumulation, as well as imaging of SAH-associated inflammation. Moreover, the detection of leptomeningeal PFCEs might give further insights into the lymphatic drainage of the SAS and central nervous system following SAH. Utilizing PFCEs may enable monitoring of the immune cell activation and blood clearance after SAH and therefore, serve as a modality to monitor therapeutic response in further translational treatment studies in SAH.

## DTI studies of the Multiple Sclerosis influence on the Uncinate Fasciculus structure using the BSD-DTI

Anna K. Stefańska[1], Sara Kierońska-Siwak[2], Artur T. Krzyżak[1]

[1]Faculty of Electrical Engineering, Automatics, Computer Science and Biomedical Engineering, AGH University of Science and Technology, Cracow, Poland. [2]Department of Neurosurgery and Neurology, Jan Biziel University No 2, Collegium Medicum, Nicolaus Copernicus University, Bydgoszcz, Poland

**Introduction**: Diffusion tensor imaging (DTI) is a non-invasive MRI technique that produce detailed images of the brain's white matter. In Multiple Sclerosis (MS), the nerve fibers become damaged, leading to a loss of their ability to transmit signals effectively[1]. The two main parameters derived from DTI are mean diffusivity (MD)[2] and fractional anisotropy (FA)[3]. In MS, the nerve fibers in the white matter become damaged. The *Uncinate Fasciculus* is a WM fiber pathway in the brain that connects the temporal lobe and the prefrontal cortex (PFC)[4]. BSD-DTI is a tool to reduce systematic errors of standard anisotropic tissues DTI.

**Methods**: DTI measurements of 10 HC and 10 *MS* were conducted on a 3T Siemens Magnetom scanner in the University Hospital in Cracow, Poland. Selected axial right and left UF ROIs were performed by the basis of DSI Studio anatomical atlas data and then convert to BSD-DTI software.

**Results**: The BSD-DTI method was used and the quality of FT improved. Neural pathways are much more precise and accurate, which means that neuronavigation will work much better, with a greater probability of mapping actual neural connections.

**Conclusion**: The reduction of systematic errors has a visible effect on the DTI and FT metrics. The reduction of systematic errors can be essential for the accurate quantitative characterization of the

brain by means of DTI. The reduction of the impact of magnetic field gradient inhomogeneities affecting DTI based tractography with the proposed approach for b-matrix spatial distribution refinement were successfully implemented in signal post processing for the refinement of human brain scans. The effect of the correction of the diffusion signal tensor is the improved graphic representation of fiber position, which resulted in the better visualization of small crossing fibers but also big bundles. More detailed and more realistic presentation of fibers is the highest goal of

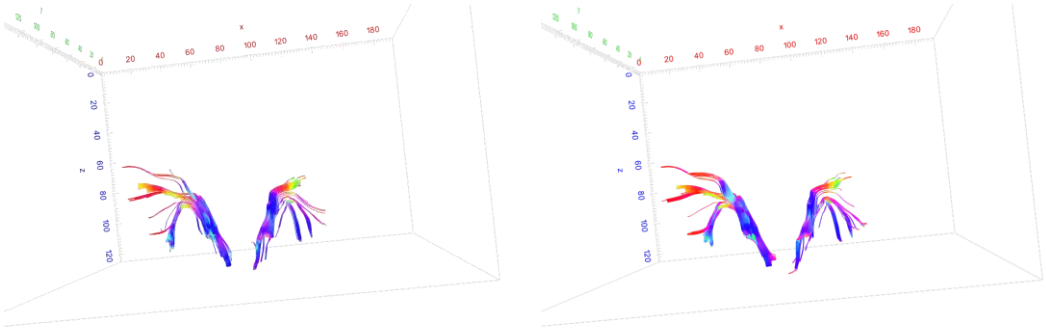

practical tractography and a step forward in the refinement of the presentation of brain fiber tracts which is important for the practical presentation of brain structure. The technique is needed and might be used as a valuable tool by medical professionals, especially neurosurgeons where mapping precision is vital in surgical planning.

References:
1. Roosendaal S, et al. Regional DTI differences in multiple sclerosis patients. Neuroimage 2009.
2. Basser P, et al. Microstructural and Physiological Features of Tissues Elucidated by Quantitative-Diffusion-Tensor MRI. Journal of Magnetic Resonance 1996.
3. Özarslan E, et al. Generalized scalar measures for diffusion MRI using trace, variance, and entropy. Magnetic Resonance in Medicine 2005.
4. Hulst H, et al. Cognitive impairment in MS Impact of white matter integrity, gray matter volume, and lesions From the Departments of Radiology. American Academy of Neurology 2013.

## Non-invasive determination of oxygen partial pressure in ischemic tissue by $^{19}$F MR relaxometry

Nicolas Stumpe[1], Tuba Güden-Silber[1], Rebekka Schneckmann[2], Katharina Wolters[2], Maria Grandoch[2], Ulrich Flögel[1]

[1]Institute for Molecular Cardiology, Heinrich Heine University, Düsseldorf, Germany; [2]Institute for Translational Pharmacology, Heinrich Heine University, Düsseldorf, Germany

Circulatory disorders and the hypoxia they cause in organs are among the most frequent causes of death in industrialized countries. However, methods for non-invasive assessment of tissue oxygen level are lacking. The use of physiologically inert perfluorocarbon nanoemulsion (PFC) offers a potential solution for noninvasive determination of tissue partial pressure of oxygen ($pO_2$) using fluorine magnetic resonance imaging ($^{19}$F MRI). The method exploits the property of PFCs that they dissolve oxygen in proportion to the ambient $pO_2$, which leads to a linear change in the $^{19}$F relaxation rate $R_1$[1]. To acquire the $^{19}$F $T_1$ relaxation times a flow sensitive alternating inversion recovery echo planar imaging sequence (FAIR-EPI) at 9.4T was used. A 20% perfluoro-15-crown-5 ether nanoemulsion[2] was used to record the relation between the relaxation rate $R_1 = 1/T_1$ to the surrounding $pO_2$ and the temperature in a three-dimensional surface-plot. $^{19}$F MR relaxometry was applied to determine tissue $pO_2$ in a murine hindlimb ischemia model (HLI)[3]. For this purpose, an occlusion was placed at the femoral artery in the left hind leg. To examine $pO_2$, 100 µl of PFCs were injected bilaterally into the muscles of the upper legs and 50 µl into the lower leg. FAIR-EPI sequence was used to quantify $^{19}$F $T_1$ for the ischemic and control hindlimb one day after surgery. Optimization of the sequence, by rescaling the trajectories of $^{1}$H reference scans, ghosting artefacts for $^{19}$F scans could be eliminated. Through the phantom experiments, a linear relationship was found between $^{19}$F relaxation rate $R_1$ to $pO_2$ and temperature. In the in vivo experiments, the sham hindlimb

showed a $pO_2$ of 31.2+7.2 mmHg (n=9). A significant decrease of $pO_2$ to 13.0+6.9 mmHg could be found in the ischemic upper leg. In the experiments of the carves a similar $pO_2$ was found for the sham hindlimb (29.3+10.9 mmHg, n=3), while the $pO_2$ in the ischemic hindlimb decreased even further (6.8+13.9 mmHg, n=3). The values measured in this study are in the same range as the literature values. In conclusion, the non-invasive method of determining partial pressure of oxygen using $^{19}F$ MR relaxometry offers a good alternative to the previous highly invasive methods. This has been demonstrated in the example of a murine hind limb ischemia model. Since similar PFCs have already been investigated in clinical studies, clinical translation of the method is highly promising.

References:
1. Chapelin F et al. Prognostic value of fluorine-19 MRI oximetry monitoring in cancer. Mol Imaging Biol. 2022;24(2):208-219.
2. Flögel U et al. In vivo monitoring of inflammation after cardicac and cerebral ischemia by fluorine magnetic resonance imaging. Circulation 2008;118(2):140-148.
3. Schneckmann R et al. Endothelial hyaluronan synthase 3 augments postischemic arteriogenesis through CD44/eNos signaling. Arterioscler Thromb Vasc Biol. 2021;41(10):2551-2562.

# Posters

**MRI-based in vivo detection of the early changes in vascular phenotype in murine models**

Anna Bar[1], Brygida Marczyk[1,2], Anna Grochot-Przęczek[3], Stefan Chłopicki[1,2]

[1]Jagiellonian University, Jagiellonian Centre for Experimental Therapeutics (JCET), Krakow, Poland; [2]Jagiellonian University Medical College, Faculty of Medicine, Chair of Pharmacology, Krakow, Poland; [3]Jagiellonian University, Department of Medical Biotechnology, Faculty of Biochemistry, Biophysics and Biotechnology, Kraków Poland

**Background:** Endothelial dysfunction (ED) is a hallmark of vascular disorders, in various diseases and has pathophysiological, prognostic and therapeutic significance. Therefore, the ED assessment in vivo, in clinically relevant animal models, is essential for better understanding of the endothelium role in the disease progression and of the novel pharmacotherapeutic mechanisms efficacy, in the treatment of ED in vivo. Currently, various tests are used for endothelial phenotyping, but most of them are not sensitive to detect the early phase of ED.

**Methods and results:** In the present study, endothelial phenotyping was performed as multifactorial assessment with MRI in vivo in comparison to nitric oxide production measurements with EPR in the aorta ex vivo and to USG-Doppler-based assessment of arterial stiffness, in 3- and 6-7-month-old mice with endothelial-specific knockout of nuclear factor 2 ($Nrf2^{flox}$xVE-cad-CRE+). While, in 6-month-old $Nrf2^{flox}$xVE-cad-CRE+ mice arterial stiffness, measured as pulse wave velocity and nitric oxide production were not changed in the aorta, MRI-based assessment revealed impaired acetylcholine-induced response in the aorta, with preserved endothelium-independent response to sodium nitroprusside and impaired flow-mediated response in the femoral artery. Moreover, it was demonstrated, that changes in the endothelial permeability, assessed by MRI with the use of gadolinium-loaded liposomes, were detected in the femoral artery, brachiocephalic artery and aorta in 3-month-old $Nrf2^{flox}$xVE-cad-CRE+ mice.

**Conclusions:** MRI-based assessment of systemic endothelial phenotype in vivo is suitable for detecting early changes in vascular wall pathology in murine models of ED in vivo. In particular, assessment of the changes in endothelial permeability allow for the detection very early changes preceding changes in endothelial function, considered as the most sensitive to this date. Altogether, results of this study may open up new perspectives for early ED diagnosis and research on endothelium-targeted pharmacotherapy in murine models in vivo.

Acknowledgements:
This work was supported by the Polish National Science Centre (NCN) grant: OPUS No 2020/39/B/NZ5/02305.

**3D printed pharmaceutical dosage forms and wound dressings studied by MRI methods**

Ewelina Baran[1], Piotr Kulinowski[1]

[1]Institute of Technology, University of the National Education Commission, Kraków, Poland

The future of medicine will likely turn to personalized medicine to tailor treatment to individual needs. Current pharmaceutical production is not suitable for personalized medical devices. Over the last few years, a rapid increase in interest in 3D printing in the pharmaceutical field has been observed [1], especially in technologies such as selective laser sintering (SLS) and the 3D Vat Polymerization. Understanding the physicochemical processes occurring during the printing and drug release process of pharmaceutical products can help in their rational design. MRI methods allow for the assessment of mass transport phenomena at the molecular and macro levels, without disturbing the processes occurring inside the material [2, 3].

Pharmaceutical matrices containing various proportions of PEGDA/PEG and additives known from tableting with a low dose of ropinirole or metronidazole as the active substance (drug) were prepared by vat photopolymerization. High-dose tablets were also

prepared using the SLS method (with metronidazole as API). In vitro pharmaceutical properties (i.e. in vitro drug release) were obtained. These results were complemented by in situ magnetic resonance imaging. The bidirectional mass transport of mobile phases in DLP-printed matrices (i.e. PEG and water) was assessed. It was found that the observed phenomena are related to functional and pharmaceutical properties. It has been shown that using H2O and D2O as hydration (dissolution) media, it is possible to assess phenomena related to the evolution of the material originally contained in the matrix (polymer chains and water molecules strongly bonded to them).

Acknowledgements:
The work was supported by the National Science Centre Poland grant number UMO-2022/45/B/NZ7/04081.

References:

1. A. Awad, S. J. Trenfield, S. Gaisford and A. W. Basit, International Journal of Pharmaceutics, 2018, 548, 586-596.
2. P. Kulinowski, K. Woyna-Orlewicz, G.-M. Rappen, D. Haznar-Garbacz, W. P. Weglarz and P. P. Dorozynski, International Journal of Pharmaceutics, 2015, 484, 235-245.
3. E. Baran, A. Birczyński, P. Dorożyński and P. Kulinowski, Carbohydrate Polymers, 2023, 299, 120215.

## Molecular Magnetic Resonance Imaging of Prostate Cancer using Targeted Core/Shell Nanoparticles

Armita Dash[1], Fong-Yu Cheng[2], Krzysztof Jasinski[3], David MacDonald[3], Boguslaw Tomanek[3,4,5], Frank C. J. M. van Veggel[1], Barbara Blasiak[3,5]

[1]Department of Chemistry, University of Victoria, British Columbia, Victoria, Canada; [2]Department of Chemistry, Chinese Culture University, Taipei, Taiwan; [3]Polish Academy of Sciences, Institute of Nuclear Physics, Krakow, Poland; [4]University of Alberta, Department of Oncology, Edmonton, Canada; [5]Department of Clinical Neurosciences, University of Calgary, Calgary, Canada

After lung cancer, prostate cancer (PC) is the most common and the second leading cause of cancer death (1). Currently, the gold standard for PC diagnosis is prostate-specific antigen (PSA) testing and digital rectal examination (2). Computed Tomography, Positron Emission Tomography (3) etc. are used for PC diagnosis and staging, yet they are of limited value. Molecular MRM using targeted contrast agents may rectify limitations of these methods.

To improve the tumor contrast we have developed new core/shell $NaDyF_4/NaGdF_4$ nanoparticles changing both $T_1$ and $T_2$ relaxation times of surrounding water molecules and conjugated them with tumor specific antibodies and proteins. We also investigated toxicity, biodistribution and clearance of the new contrast agent. The relaxation times ($T_1$ and $T_2$) of the nanoparticles with various core/shell sizes and concentrations were measured at 9.4T. We performed in vivo imaging using mouse model of cancer and used 9.4T MRI system. We imaged nude mouse with the tumor before and after the injection of targeted and non-targeted contrast agents.

Our results show that the new contrast agents may allow earlier detection of cancerous tissues than standard $T_1$- or $T_2$-only contrast.

Acknowledgments:
This work was funded by the National Science Center, Poland Grant numbers: Harmonia: 2018/30/M/NZ5/00844.

References:

(1) http://www.cancer.org/cancer/prostatecancer.
(2) http://www.cancer.ca/Canada-wide.
(3) H. Carter, L. Ferrucci, A. Kettermann, P. Landis, E. Wright, J. Epstein, B. Trock and J. Metter, "Detection of Life-Threatening Prostate Cancer With Prostate-Specific Antigen Velocity During a Window of Curability," Journal of the National Cancer Institute, vol. 98(21), pp. 1521-1527, 2006.

## Visualisation of Pancreatic Islets transplanted into the greater omentum using an ECM skeleton as a supportive structure

David Červený[1], Zuzana Berková[1], František Saudek[1], Kateřina Sulková[1], Dominik Havlíček[1], Vilém Neděla[2], Daniel Jirák[1]

[1]Institute for Clinical and Experimental Medicine, 14021 Prague, Czech Republic; [2]Environmental Electron Microscopy Group, Institute of Scientific Instruments, The Czech Academy of Sciences, 61264 Brno, Czech Republic

Infusing pancreatic islets into the liver through portal vein currently represents the preferred approach for islet transplant site, despite considerable loss of islet mass almost immediately after implantation. Therefore, new approaches that obviate direct intravascular placement are urgently needed. A promising candidate for extrahepatic placement is the omentum. We aimed to develop an extracellular matrix skeleton from the native pancreas that could provide a microenvironment for islet survival in an omental flap. Pancreatic perfusion via the splenic vein provided smaller extracellular matrix skeletons, which facilitated transplantation into the omentum, without compromising other requirements, such as the complete depletion of cellular components and the preservation of pancreatic extracellular proteins. Repeated MR imaging of iron-oxide-labeled pancreatic islets showed that islets maintained their position in vivo for a long period. Advanced environmental scanning electron microscopy demonstrated that islets remained integrated with the pancreatic skeleton. This novel approach represents a proof-ofconcept for long-term transplantation experiments. We have although found out, that the ironoxide nanoparticles are not ideal for this new transplant site due to the non-homogenous nature of peritoneal cavity, and therefore the low specificity of this method. Therefore, we have paid attention to $^{19}F$ labels and utilizing $^{19}F$ MRI methods. To address drawback with lower sensitivity and the labelling efficiency. we have further explored and optimized the labelling process using an optimized pre-microporation method developed in our lab. We have also manufactured more sensitive coils specific for the application. Our goal is to repeat the experiment while monitoring the transplanted pancreatic islets by $^{19}F$ MRI.

Acknowledgements:
This project was supported by the Czech Ministry of Health (NU22-08-00286).

References:

Berkova Z, Zacharovova K, Patikova A, Leontovyc I, Hladikova Z, Cerveny D, Tihlarikova E, Nedela V, Girman P, Jirak D, Saudek F. Decellularized Pancreatic Tail as Matrix for Pancreatic Islet Transplantation into the Greater Omentum in Rats. J Funct Biomater. 2022 Sep 30;13(4):171. doi: 10.3390/jfb13040171. PMID: 36278640; PMCID: PMC9589982.

## Methodological issues of manganese-enhanced resonance imaging (MEMRI) and practical applications

Monika Drabik[1,2] , Michał Wieteska[1,2], Marlena Wełniak-Kamińska[1], Piotr Bogorodzki[1,2]

[1]Mossakowski Medical Research Institute, Polish Academy of Sciences, Warsaw, Poland; [2]Faculty of Electronics and Information Technology, Warsaw University of Technology, Warsaw, Poland

Manganese-enhanced magnetic resonance imaging (MEMRI) is a powerful tool for preclinical studies of brain-wide physiology in awake-behaving animals. This technique is based on the physicochemical and biological properties of manganese ions ($Mn^{2+}$). As they have similar ionic radius as calcium ions, they can behave as $Ca^{2+}$ analogue and selectively enter active neurons via membrane voltage-gated $Ca^{2+}$ channels. Moreover, due to its paramagnetic nature, $Mn^{2+}$ shortens the spin-lattice relaxation time ($T_1$) of water protons that were exposed to manganese ions and, consequently, enhanced contrast in active regions is observed [1]. These characteristics make MEMRI a promising tool with a wide range of applications in neuroscience and other related fields.

As manganese has toxic properties, doses must be relatively low. Depending on the route of manganese administration and the type of experiment design (e.g. the kind of animal model, the frequency of administration and the type of external stimulus applied to the animals), different information might be obtained based on induced accumulation of manganese ions. Taking advantage of active axonal transport of $Mn^{2+}$, MEMRI has also been used as a tract tracer for the neuronal pathways, including the visual, olfactory, auditory, and sensory pathways after the activation of the corresponding sense.

The goal of this work is to demonstrate our findings regarding MEMRI technique. We explored different routes of manganese administration, such as nasal, intraperitoneal and intravitreal.

References:
1. Uselman TW, Medina CS, Gray HB, Jacobs RE, Bearer EL. Longitudinal manganese-enhanced magnetic resonance imaging of neural projections and activity. NMR Biomed. 2022 Jun;35(6):e4675. doi: 10.1002/nbm.4675. Epub 2022 Mar 6. PMID: 35253280.
2. Fiedorowicz M, Orzel J, Kossowski B, Welniak-Kaminska M, Choragiewicz T, Swiatkiewicz M, Rejdak R, Bogorodzki P, Grieb P. Anterograde Transport in Axons of the Retinal Ganglion Cells and its Relationship to the Intraocular Pressure during Aging in Mice with Hereditary Pigmentary Glaucoma. Curr Eye Res. 2018 Apr;43(4):539-546. doi: 10.1080/02713683.2017.1416147. Epub 2017 Dec 28. PMID: 29283693.

**MR-based phenotyping reveals early lipodystrophy in diet-induced obesity**

Vera Flocke, Katja Wegener, Tamara Straub, Maria Grandoch, Ulrich Flögel

University Hospital Düsseldorf, Institute for Molecular Cardiology, Düsseldorf, Germany

**Introduction:** Obesity is one of the main risk factors for type 2 diabetes and is also associated with an increased cardiovascular risk [1,2]. However, the transition from the early states of impaired glucose intolerance to a more progressive disease stage still remains elusive [3]. Thus, in the present study, we used mice exposed to a high fat/carbohydrate diet to characterize the temporal development of alterations in different organs by comprehensive MRI/MRS phenotyping in order to identify time points, where therapeutic interventions might stop further transition.

**Methods:** Male (8-10w) C57BL/6J mice were fed a HFD for 9 weeks while control animals received a matching chow diet. Body weight and fasting blood glucose were determined by intraperitoneal glucose tolerance test. Furthermore, *in vivo* $^{1}$H MRS was used to determine every 3 weeks the lipid content in heart (PRESS, TAcq 17 min, 1024 avg., 256 data pts., voxel size 1x2x3 mm), the extra- and intramyocellular lipids in *M. tibialis a.* (PRESS, TAcq 18 min., 1024 avg., 2048 data pts., voxel size 1.3x1.3x3 mm) and the lipid content of the liver (PRESS, TAcq 4 min., 256 avg., data pts. 2048, voxel size 2mm$^3$).

**Results:** Feeding with HFD led to a strong weight gain and the fasting glucose levels were also significant different after 6 weeks. At the tissue level, this was accompanied by a significant elevation of cardiac lipids after six weeks in the HFD-fed animals. However, in the M. tibialis anterior we found already after 3 weeks a significant und substantial increase of muscle lipids in the HFD group. Due to the anatomical structure of the muscle fibers, it is further possible to distinguish IMCL from EMCL. Interestingly, IMCL exhibited a massive increase after 3 weeks of HFD, staying almost constant thereafter, while EMCL increased steadily over time. These early alterations in skeletal and cardiac muscle were also associated with a significant hepatosteatosis after 3 weeks of feeding.

**Conclusion:** Using the diet-induced obesity model we could detect massive accumulation of lipids in all organs studied already at time points, where body weight of mice was not yet altered. Importantly, $^{1}$H MRS was most sensitive to reveal *in vivo* very early alterations in tissue properties in this prediabetic state. It, thus, may also be used in humans to identify patients at the transition point from prediabetes to diabetes.

References:
1. C. A. Maggio und F. X. Pi-Sunyer, „Obesity and type 2 diabetes“, Endocrinol. Metab. Clin. North Am., Bd. 32, Nr. 4, S. 805–822, Dez. 2003, doi: 10.1016/S0889 8529(03)00071-9.
2. A. Melmer, P. Kempf, und M. Laimer, „The Role of Physical Exercise in Obesity and Diabetes“, Praxis, Bd. 107, Nr. 17–18, S. 971–976, Aug. 2018, doi: 10.1024/16618157/a003065.
3. L. La Sala und A. E. Pontiroli, „Prevention of Diabetes and Cardiovascular Disease in Obesity“, Int. J. Mol. Sci., Bd. 21, Nr. 21, S. E8178, Okt. 2020, doi: 10.3390/ijms21218178.

**Comparison of two software packages to analyze preclinical dynamic contrast-enhanced MRI data to evaluate the angiogenic status of the tumor microenvironment in a xenograft breast cancer model**

Joachim Friske[1], Silvester J. Bartsch[1], Daniela Laimer-Gruber[1], Thomas Wanek[1], Claudia Kuntner-Hannes[1], Thomas H. Helbich[1], Katja Pinker[1,2]

[1]Division of Structural and Molecular Preclinical Imaging (PIL), Department of Biomedical Imaging and Image-Guided Therapy, Medical University of Vienna, Vienna, Austria; [2]Breast Imaging Service, Department of Radiology, Memorial Sloan Kettering Cancer Center, New York, NY, USA

Angiogenesis, the formation of new blood vessels, is vital for supplying the growing tumor with oxygen and nutrients. Angiogenesis can be studied by using dynamic-contrast-enhanced (DCE) magnetic resonance imaging, where a gadolinium-based contrast agent is used to probe the vascular tumor microenvironment. Quantitative analyses are performed using pharmacokinetic models to calculate the tumor plasma volume fraction ($v_p$), extravascular volume fraction ($v_e$), and the volume transfer constant ($K_{trans}$). Several software packages are available for clinical application however most of them cannot be directly used with preclinical data. We found that an open-source MATLAB implementation for the analysis of DCE data called ROCKETSHIP[1] can be adapted to suit our specific needs. In addition to that, we also used the commercially available software PMOD (V4.3). For each software, we develop a postprocessing protocol to standardize our quantitative analysis of our preclinical DCE data. DCE measurements on tumor-bearing female athymic nude mice were performed using a 9.4T (Bruker BioSpec 94/30USR) MRI system equipped with a 35 mm $^1$H volume coil (Bruker, Germany). For $T_1$ correction first a $T_1$-map was measured using a RARE sequence (TE=28ms, TR=200-6000ms 12 steps, RF=8, SL=1mm, FOV35x35mm, Matrix 128x128) followed by a FLASH sequence for DCE-MRI acquisitions (TE=1.8ms, TR=10ms, FA=15, SL=1mm, FOV35x35mm, Matrix 128x128, 600 Rep). After 2 min of baseline imaging, a bolus of 0.2 mM/kg gadopentetate dimeglumine (Magnevist) was administered using a syringe pump. Additionally, a small group ($n$ = 4) of non-tumor bearing animals was measured using the same setup for the generation of a population-based arterial input functions (AIF). Both software packages show similar results for $v_p$, $v_e$, and $K_{trans}$ using the measured $T_1$-map and AIF applying the Ex-Tofts model. While ROCKETSHIP is the more flexible software allowing own adoptions PMOD has the more advanced graphical toolbox and a large toolbox for pharmacokinetic models.

References:
1. Barnes SR, Ng TS, Santa-Maria N, Montagne A, Zlokovic BV, Jacobs RE. ROCKETSHIP: a flexible and modular software tool for the planning, processing and analysis of dynamic MRI studies. BMC Med Imaging. 2015 Jun 16;15:19.

**Fluorinated Nanoparticles as Theranostic Platform for $^{19}$F MRI**

Dominik Havlicek[1], Vyshakh M. Panakkal[2], Ondrej Sedlacek[2], Daniel Jirak[1]

[1]Department of Diagnostic and Interventional Radiology, Institute for Clinical and Experimental Medicine, Prague, Czech Republic; [2]Department of Physical and Macromolecular Chemistry, Faculty of Science, Charles University, Prague, Czech Republic

Theranostics provide information about diagnostics and enable therapy, thereby providing new prospects for overcoming limitations of traditional treatments. In this context, perfluorocarbons (PFCs) are the most widely used tracers in preclinical fluorine-19 magnetic resonance ($^{19}$F MR), primarily for their high fluorine content. However, PFCs are extremely hydrophobic, and their solutions often display reduced biocompatibility, relative instability, and subpar $^{19}$F MR relaxation times [1]. This study aims at exploring the potential of micellar $^{19}$F MRI tracers, synthesized by polymerization-induced self-assembly (PISA) [2,3], as alternative theranostics agents for simultaneous imaging and release of the non-steroidal antileprotic drug clofazimine. We proved that these micelles demonstrate sustained drug release i*n vitro*, under physiological conditions. Throughout the drug release process, they provide a highly specific and sensitive *in vivo* $^{19}$F MR

imaging (MRI) signal. Even after extended exposure, these fluoropolymer tracers show biocompatibility, as confirmed by our histological analysis. Moreover, the characteristics of these polymers can be broadly adjusted to meet the wide range of criteria for preclinical and clinical settings. Therefore, micellar $^{19}$F MRI tracers display physicochemical properties suitable for *in vivo* imaging, and high performance as drug carriers, highlighting their potential as both diagnostic and therapeutic tools.

References:
1. Jirak, D.; Galisova, A.; Kolouchova, K.; Babuka, D.; Hruby, M. Fluorine Polymer Probes for Magnetic Resonance Imaging: Quo Vadis? *Magn Reson Mater Phy* **2019**, *32* (1), 173–185.
2. Panakkal, V. M.; Havlicek, D.; Pavlova, E.; Filipová, M.; Bener, S.; Jirak, D.; Sedlacek, O. Synthesis of $^{19}$ F MRI Nanotracers by Dispersion Polymerization-Induced SelfAssembly of *N* -(2,2,2-Trifluoroethyl)Acrylamide in Water. *Biomacromolecules* **2022**, *23* (11), 4814–4824.
3. Canning, S. L.; Smith, G. N.; Armes, S. P. A Critical Appraisal of RAFT-Mediated Polymerization-Induced Self-Assembly. *Macromolecules* **2016**, *49* (6), 1985–2001.

**A temperature-controlled NMR head for diffusion and relaxation measurements of water solutions of superparamagnetic particles (SPM) in low field MRI scanner**

Karolina Janiszewska, Grzegorz Domański, Wojciech Obrębski, Mateusz Midura, Michał Wieteska, Piotr Bogorodzki

Institute of Radioelectronics and Multimedia Technology, Warsaw University of Technology, Warsaw, Poland

Superparamagnetic (SPM) nanoparticles, thanks to their great magnetization, induce great variations in the proton relaxation times that affect magnetic resonance image (MRI) contrast. A complete understanding of this phenomenon [1] requires temperature-controlled either relaxation or diffusion measurements.

The goal of this work was to design and validate a NMR head with variable temperature control designed to work inside a Philips Outlook ProView MRI scanner with main field of 0.23T, which corresponds to Larmor frequency of 9.8MHz. The scanner B0 field orientation determines the type of resonator. Vertical systems use a solenoid coil, Helmholtz, scroll-coil or loop-gap; however, from all axial resonators, solenoid has been repeatedly reported as an optimal solution whenever possible [2,3]. In our setup solenoidal coil made from copper pipe (1mm ID) had a diameter of 20mm and length of 52mm and is intentionally intended for small 2-5ml vials. An external refrigerated circulator (Thermo Scientific™ ARCTIC A10) was used to circulate water at variable temperature through the coil turns. Thanks to thermal insulation of the coil with Styrofoam and the use of a fiber-optic thermometer (LTX-300-LUX+, OSENSA Innovations), the temperature of the liquid in the sample was kept under control. Inversion Recovery (IR), Carr-Purcell-Meiboom-Gill (CPMG) and Pulsed Gradient Spin Echo,

(PGSE) sequences were implemented on additional (Kea2, Magritek) to manufacturer's (Outlook, ProView, Philips) MRI console under PROSPA software environment (Magritek). $T_1$, $T_2$ relaxation and diffusion measures were calculated 'on-line' under PROSPA. To ensure correct positioning of the coil system in relation to geometrical center of the magnet, a support was designed, that improved the final homogeneity obtained within the sample. Finally, the system was validated on a set of test solutions at variable temperatures and the resulting measurements were consistent with the theoretical values.

References:
1. A. Roch, R.N. Muller, P. Gillis, Theory of proton relaxation induced by superparamagnetic particles, J. Chem. Phys. 110 (11) (1999), 5403-5411.
2. D. I. Hoult i R. E. Richards, „The signal-to-noise ratio of the nuclear magnetic resonance experiment", J. Magn. Reson., t. 213, nr 2, ss. 329–343, 2011.
3. C. M. de Miranda i S. F. Pichorim, „Self-resonant frequencies of air-core single-layer solenoid coils calculated by a simple method", Electr. Eng., t. 97, nr 1, ss. 57–64, 2014.

**Black and green tea from the NMR point of view**

Teobald Kupka[1], Natalina Makieieva[1], Joanna Nackiewicz[1], Barbara Blicharska[2], Magdalena Witek[3]

[1]Opole University, Faculty of Chemistry, 45-052 Opole, Poland; [2]Jagiellonian University, Faculty of Physics, Astronomy and Applied Computer Science, 30-348 Kraków, Poland; [3]University of Agriculture in Krakow, 30-149 Kraków, Poland

Hot water infusion from tea leaves is considered one of the most popular drinks worldwide. Its beneficial impact on human body is related to the presence of a large number of bioactive compounds present in water extract. These compounds, as monitored by UV-VIS spectroscopy, are mainly well dissolved in hot water. Among the highly abundant compound is caffeine (theine). It is well soluble in hot water and, upon cooling of freshly prepared tea drink, it forms a very thin layer on its surface. On the other hand, oxygen dissolution in hot tea is very limited but increases with temperature lowering. The presence of numerous compounds exhibiting “free radical scavenger” activity is considered beneficial to human. The ability to deactivate free radicals is correlated to the presence of easily oxidized polyphenols. However, their concentration in hot tea drink decreases with time. On the other hand, the presence of free radicals decreases relaxation time $T_1$ of water signal in $^{1}H$ NMR spectrum[1]. Thus, water signal can be used as a ‘probe’ of free radical presence in tea. Interestingly, only $^{1}H$, $^{13}C$ and $^{15}N$ NMR data for caffeine are available in the literature and no $^{17}O$ NMR spectra are reported[2]. As continuation of our earlier works on natural bioactive compounds [3-5], using molecular modeling at DFT level of theory, we predicted structural parameters, absolute isotropic nuclear magnetic shielding for all nuclei, chemical shifts and some indirect spin-spin coupling constants of caffeine. This could help in caffeine signals assignment of multinuclear NMR spectra of various types of tea.

References:

1. J. van Duynhoven, A. Voda, M. Witek, H. Van As, Time-domain NMR applied to food products, Annual Reports on NMR Spectroscopy, 2010, pp. 145-197.
2. J. Sitkowski, L. Stefaniak, L. Nicol, M.L. Martin, G.J. Martin, G.A. Webb, Spectrochimica Acta Part A: Molecular and Biomolecular Spectroscopy, 51 (1995) 839-841.
3. P. Najgebauer, M. Staś, R. Wrzalik, M.A. Broda, P.P. Wieczorek, V. Andrushchenko, T. Kupka, Journal of Molecular Liquids, 363 (2022) 119870.
4. T. Kupka, P.P. Wieczorek, Spectrochimica Acta Part a-Molecular and Biomolecular Spectroscopy, 153 (2016) 216-225.
5. N. Makieieva, T. Kupka, G. Spaleniak, O. Rahmonov, A. Marek, A. Błażytko, L. Stobiński, N. Stadnytska, D. Pentak, A. Buczek, M.A. Broda, P. Kuś, J. Kusz, M. Książek, Structural Chemistry, 33 (2022) 2133-2145.

**Gadolinium labeled polyelectrolyte nanocapsules for drug delivery and MRI detection – MR investigation of the influence of shell composition on contrasting properties**

Natalia Łopuszyńska[1], Krzysztof Szczepanowicz[2], Marta Szczęch[2], Krzysztof Jasiński[1], Kamil Stachurski[1], Katarzyna Kalita[1], Piotr Warszyński[2], Władysław P. Węglarz[1]

[1]Institute of Nuclear Physics Polish Academy of Sciences, Cracow, Poland;
[2]Institute of Catalysis and Surface Chemistry Polish Academy of Sciences, Cracow, Poland

Modification of polymeric nanocarriers with imaging agents introduces the possibility of the observation of drug kinetics and the assessment of the efficiency of the therapeutics' transport to the site of action. The present contribution aimed to investigate the possibility of the detection of new theranostic polyelectrolyte nanocarriers modified with Gd compound (Gd-PLL) via Magnetic Resonance Imaging (MRI). In particular, the influence of a number of Gd-PLL layers in nanocapsules' shell on the contrasting properties of the construct was assessed.

Various types of nanocarriers were formed via the layer-by-layer technique, i.e., by the deposition of ionic and cationic polyelectrolyte shell layers on nanoemulsion drops. The core of nanocarriers was either polymeric (PCL) or nanoemulsion-type (AOT/PLL), while

the MRI contrast agent (PLL-Gd) formed one or two layers of the nanocarrier shell. Both the $^{1}$H MR relaxation measurements and MR imaging were performed at the 9.4T BioSpec 94/20 preclinical MRI scanner (Bruker BioSpin, Germany), equipped with BGA60-S gradient coils and a 35 mm birdcage RF coil, controlled by Paravision 6 software.

All the investigated nanocarriers exhibited decent MRI properties. In particular, values of $r_1$ molar relaxivities were in the range of 2.53 to 3.71 $mM^{-1}s^{-1}$, which is very similar to commercially used contrast agents. The values of $r_2$ molar relaxivities were in the range of 11.9–22.8 $mM^{-1}s^{-1}$, which will introduce only slight $T_2$ contrasting. Surprisingly, the molar relaxivities of nanocarriers with one and two layers of PLL-Gd were in the same range. However, analysis of the obtained results with respect to the concentration of the whole nanocarriers highlights the versatility of synthesized compounds. By increasing the number of layers of PLL-Gd, $R_1$-contrasting properties can be further enhanced. On the other hand, a similar effect can be achieved by increasing the total number of NCs with only a single layer of PLL-Gd, allowing a higher concentration of therapeutic agents to be delivered.

Acknowledgements:
This work was supported by the National Centre of Science (NCN) of Poland, grant nr: 2019/34/H/ST5/00578 (GRIEG-1, funded under the Norwegian Financial Mechanism).

**Contrasting properties of hybrid nanosilica and cerium oxide nanoparticles for potential theranostic applications**

Natalia Łopuszyńska[1], Kamil Stachurski[1], Terje Didriksen[2], Juan Yang[2], Anna Lind[2], Sacha Muller[2], Magdalena Regulska[3], Monika Leśkiewicz[3], Magdalena Procner[3], Krzysztof Jasiński[1], Władysław Lasoń[3], Piotr Warszyński[4], Władysław P. Węglarz[1]

[1]Institute of Nuclear Physics Polish Academy of Sciences, Cracow, Poland; [2]SINTEF Industry, Department of Process Technology, Oslo, Norway; [3]Maj Institute of Pharmacology Polish Academy of Sciences, Cracow, Poland; [4]Institute of Catalysis and Surface Chemistry Polish Academy of Sciences, Cracow, Poland

The aim of the present study was to evaluate the MRI contrasting properties of a series of new nanoparticles that can be classified into two categories: HNS (Hybrid Nanosilica)-based nanoparticles (NPs): HNS, HNS-Gd, lactamide-HNS-Gd, $^{19}$F-HNS and ceria-based NPs: $CeO_2$ and $CeO_2$-Gd. While the ceria nanoparticles have already been investigated for their neuroprotective effect, HNS can be easily further functionalized for theranostic purposes.

For the Gd-based nanoparticles, contrasting properties were investigated by the measurement of molar relaxivities $r_1$ and $r_2$ and by the contrast assessment in $T_1$- and $T_2$-weighted images. The specific molar relaxivities $r_1$ results of HNS NPs were as follows: 2.12 $mM^{-1}s^{-1}$ (HNS-Gd in PBS), 0.0012 $mM^{-1}s^{-1}$ (HNS in PBS), 2.49 $mM^{-1}s^{-1}$ (Lactamide HNS-Gd), and 1.88 $mM^{-1}s^{-1}$ (HNS-Gd in water). Interestingly**,** HNS-Gd in PBS exhibited a relatively high $r_2$ value of 105.03 $mM^{-1}s^{-1}$, which can be attributed to binding to PBS particles and the creation of large molecules. Such a nanoparticle solution showed strong cytotoxic properties, while a similar effect was not observed for HNS-Gd in water. Modification of HNS-Gd with lactamide suppressed the $T_2$ effect ($r_2$ = 6.77 $mM^{-1}s^{-1}$ for lactamide-HNS-Gd) and significantly lowered cytotoxicity. Regarding $CeO_2$-based nanoparticles, MR relaxation results showed that the contrasting properties of $CeO_2$-Gd nanoparticles arise almost entirely from the presence of Gd ($r_1$ = 0.75 $mM^{-1}s^{-1}$ for $CeO_2$). $CeO_2$-Gd nanoparticles have excellent positive contrasting properties, as described by the very high $r_1$ value of 32 $mM^{-1}s^{-1}$, which was also greatly visible in MR images. $CeO_2$-Gd were non-toxic in the whole analyzed concentration range. Moreover, in the experiment with 0.5 mM $H_2O_2$, $CeO_2$-Gd nanoparticles exhibited a neuroprotective effect.

$^{19}$F-HNS exhibits preferable characteristics for $^{19}$F MRI, i.e. it has a $^{19}$F NMR spectrum with a single peak and relatively short $T_1$ relaxation time of 2.5 s and long $T_2$ time of 1.8 s.

$^{19}$F imaging was accomplished with a standard FLASH imaging sequence in a reasonable timeframe of 30 min. The SNR was around 15, which suggests that this time could be shortened, or spatial resolution increased. Moreover, $^{19}$F-HNS was non-toxic in the whole concentration range, making the proposed NPs a good candidate for further in-vivo investigations.

Acknowledgements:
This work was supported by the National Centre of Science (NCN) of Poland, grant nr: 2019/34/H/ST5/00578 (GRIEG-1, funded under the Norwegian Financial Mechanism).

**Contrast Enhancement in MRI Using Combined Double Action Contrast Agents and Image Post-Processing in the Breast Cancer Model**

David MacDonald[1], Armita Dash[2], Frank C.J.M.van Veggel[2], Boguslaw Tomanek[1,3], Barbara Błasiak[1]

[1]Institute of Nuclear Physics Polish Academy of Science, Kraków, Poland; [2]Department of Chemistry, University of Victoria, British Columbia, Canada; [3]Department of Oncology, University of Alberta, Edmonton, Canada

MRI stands out for its superior soft tissue contrast when compared to other diagnostic methods The contrast in MRI primarily determined by the relaxation times $T_1$ and $T_2$ of normal and tumor tissues. Enhancing this contrast are contrast agents that reduce $T_1$ and $T_2$ relaxation times, particularly beneficial for detecting small pathologies like early-stage breast or brain cancers [1]. Additionally, post-processing of images can further refine contrast. In our investigation, we explored changes in tumor contrast pre and post injection of non-targeted $NaDyF_4$/$NaGdF_4$ contrast. Employing image subtraction and addition techniques, we enhanced the contrast, conducting theoretical calculations using $T_1$-weighted, $T_2$-weighted, and combined images with $T_1$, $T_2$, and $T_1$/ $T_2$-targeted contrast agents in a tumor model. Imaging mice with triple-negative breast cancer and glioma tumors before and after injection of $NaDyF_4$/$NaGdF_4$ nanoparticles, using $T_1$-weighted (RARE) and $T_2$-weighted (MSME) pulse sequences on a 9.4 T MRI system, we observed a significant increase in tumor contrast through $T_2$-weighted subtracted from $T_1$-weighted images—over two-fold in the tumor model and 12% in the in vivo experiment. This suggests that image subtraction can enhance tumor contrast, potentially improving the precision of cancer detection [2].

Acknowledgements:
This work was funded by the National Science Center, Poland. Grant number: OPUS 2018/31/B/ST5/03605.

References:
[1] L. Smith et al., J. Nanomat., (2012) 1-7.
[2] D. MacDonald, A. Dash , F. C. J. M. van Veggel , B. Tomanek, B. Błasiak., MDPI., (2023), 16(8), https://doi.org/10.3390/ma16083096.

**Theoretical prediction of NMR spectra for drug delivery systems**

Natalina Makieieva[1], Teobald Kupka[1], Oimachmad Rachmonov[2] and Leszek Stobiński[3]

[1]Institute of Chemistry, University of Opole, 45-052 Opole, Poland; [2]Institute of Earth Sciences, Faculty of Natural Sciences, University of Silesia in Katowice, Sosnowiec, Poland; [3]NANOMATPL Ltd., Warsaw, Poland

Chelidonic acid is an organic compound, which occurs as a characteristic metabolite of *Chelidonium majus* L. in the natural environment. This acid is known from its therapeutic activities including analgesic, anti-inflammatory, immunomodulatory and anticancer. [1] For this reason, chelidonic acid may have great therapeutic potential in the future, and the choice of the most effective drug delivery system for its transport in the body is one of the key factors for successful therapy. In the current work, a theoretical prediction of the NMR parameters of the acid, small size models of graphene oxide as a potential carrier and non-covalent carrier-drug complexes was made. All calculations were prepared using density functional theory (DFT). Hybrid functional B3LYP with Grimme's dispersion

coefficient D3BJ and relatively accurate aug-cc-pVTZ basis set were used as most suitable methodology to predict both structural parameters and weak interactions occurring in the considered systems. [2,3] The effect of environment was provided using polarizable continuum model (PCM) for chloroform, methanol, DMSO and water solutions. [4] The obtained theoretical results suggest the possibility of formation the stable GO – chelidonic acid complex. All theoretical results were compared with available experimental data.

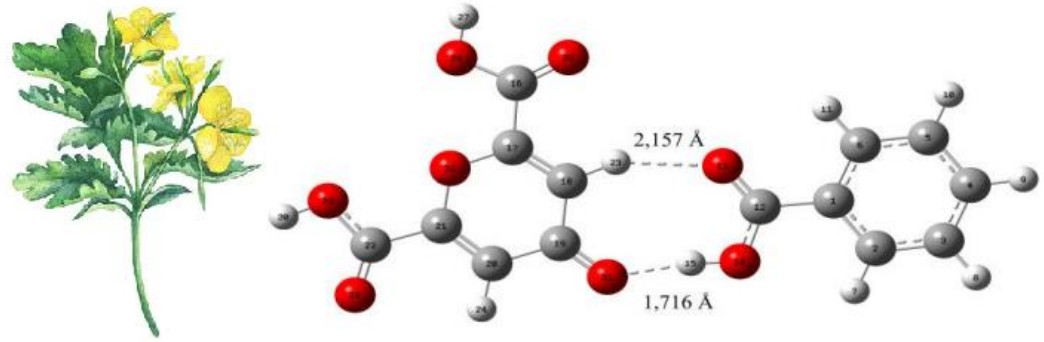


References:
1. N. Makieieva, et al., *Struct. Chem.*, 2022, 33, 2133-2145.
2. A. D. Becke A. D. *J Chem. Phys.*, 1993, 98, 5648-5652.
3. S. Grimme, et al., *J Comput. Chem.*, 2011, 32(7), 1456-1465.
4. S. Miertus, et al., *Chem. Phys.*, 1981, 55, 117-129.

## Polymeric Particles Entrapping Perfluorocarbons: A Six-Year Stability Study

Alvja Mali[1,2], Navya U. Nayak[1,2], Jessie van Doesburg[1], Remco Fokkink[3], N. Koen van Riessen[1], Robbin de Kruijf[1,4], Mangala Srinivas[1,4]

[1]Department of Cell Biology and Immunology, Wageningen University & Research, Wageningen, The Netherlands; [2]Department of Radiology, Leiden University Medical Center, Leiden, The Netherlands; [3]Department of Agrotechnology and Food Sciences, Physical Chemistry and Soft Matter, Wageningen University, Wageningen, Netherlands; [4]Cenya Imaging BV, Amsterdam, The Netherlands

Polymeric particles, particularly poly (lactic-co-glycolic acid) nanoparticles (PLGA NPs), play a pivotal role in drug delivery and serve as crucial carriers for encapsulating contrast agents used in multiple imaging techniques. Among these agents, perfluorocarbons (PFCs), synthetic organic compounds with a high payload of fluorine atoms, pose unique challenges due to their solely fluorophilic nature. However, PLGA, known for its biodegradability, biocompatibility, and FDA approval, has enabled the effective entrapment of these challenging compounds. Encapsulating PFCs within PLGA enables precise *in vivo* imaging using $^{19}$F MRI (magnetic resonance imaging), offering substantial biomedical benefits, including quantitative cell tracking and drug delivery.

PLGA-PFCE (perfluoro-15-crown-5-ether) NPs were prepared[1,2]. Subsequently, the diameter and polydispersity index (PDI) determined through Dynamic Light Scattering (DLS); and PFCE content using $^{19}$F NMR. NPs produced as early as 2016 were assessed and showed exceptional stability when stored at -20°C for a minimum of 6 years.

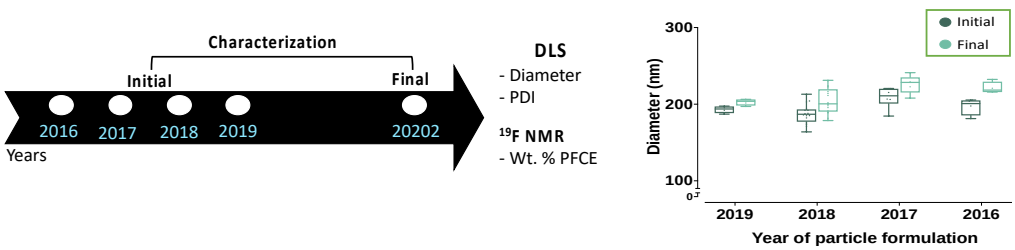


Furthermore, stability was also evaluated in both powder and suspension NPs form, with

size, PDI, and PFCE content remaining consistent throughout multiple freeze-thaw cycles. We also assessed stability at different temperatures (4°C, 37°C, and room temperature) and in various solvents, including water and serum-free medium. The NPs demonstrated stability at 4°C and room temperature across both solvents. However, at 37°C, minor diameter fluctuations were observed, likely due to the NP multi-core internal structure[1]

References:
1. Koshkina, O., et al., Multicore Liquid Perfluorocarbon Loaded Multimodal Nanoparticles for Stable Ultrasound and $^{19}$F MRI Applied to In Vivo Cell Tracking. Advanced Functional Materials, 2019. 29(19): p. 1806485.
2. Staal, A.H.J., et al., In vivo clearance of $^{19}$F MRI imaging nanocarriers is strongly influenced by nanoparticle ultrastructure. Biomaterials, 2020. 261: p. 120307.

**The impact of technical innovations on the MRI image quality**

Sebastian Plona[1,2], Henryk Figiel[2], Katarzyna Lipka[1], Jolanta Gawlińska[3]

[1]Zespół Szpitali Miejskich w Chorzowie, Zakład Radiologii, Diagnostyki Obrazowej i Medycyny Nuklearnej, Chorzów; Polska; [2]Akademia Humanitas, Instytut Nauk o Zdrowiu, Sosnowiec; Polska; [3]Tomma Diagnostyka Obrazowa S.A., Zabrze, Polska

The aim of this work is to determine the impact of technological development on improving the quality of images obtained in magnetic resonance imaging (MRI) studies. For this purpose, the information and technical documentation of two different MRI scanners produced by the same company in different years were analysed and compared: one modern and the other from a decade ago. The test images obtained on both scanners with the use of the special phantom proposed by the American College of Radiology were examined. The quality parameters of the obtained images were compared according to the criteria defined by the International Electrotechnical Commission. The analysis of the technical documentation shows that modern acquisition techniques and improvements have been implemented in the newer device. However, when examining the parameters of the images obtained with these scanners no significant improvement in the image quality was observed. It follows that in modern MRI scanners, the technological improvements do not directly affect the quality of images obtained with these devices. Technological development improves other aspects of the work with MRI scanners such as higher patient comfort, shortening of the imaging time, and broader postprocessing possibilities.

**PFCE in CX3Cr1 mice with Chronic Cranial Window after experimental Subarachnoid Hemorrhage**

Pia Pötschner[1], Anja Nitzsche[1], Felix Schoknecht[1], Philipp Boehm-Sturm[2], Peter Vajkoczy[1], Ran Xu[1]

[1]Department of Neurosurgery, Charité - Universitätsmedizin Berlin, corporate member of Freie Universität Berlin, and Humboldt-Universität zu Berlin, and Berlin Institute of Health, Berlin, Germany; [2]Department of Experimental Neurology, Charité - Universitätsmedizin Berlin, corporate member of Freie Universität Berlin, Humboldt-Universität zu Berlin, and Berlin Institute of Health, Berlin, Germany

**Background:** Secondary brain injury after Subarachnoid Hemorrhage (SAH) is one major cause for the bad outcome after the bleeding, leading to a mortality of up to 50%. Neuroinflammation is thought to be critically involved in the pathogenesis of secondary brain injury, resulting in an activation of the innate immune system after SAH. Recently it has been shown that $^{19}$F perfluoro 5-crown-15-ether (PFCE) nanoparticles label inflammatory cells via phagocytosis, enabling the tracking of immune cells after their activation. The aim of this project is the *in vivo* visualization of PFCE nanoparticles via chronic cranial window, intending to picture inflammatory cascades and clearance of immune cells after SAH.

**Methods:** We established two groups with different injection time points of the rhodamine labelled particles: after performing the chronic cranial window operation on day 0, PFCE was injected either right after the experimental SAH or one day before. SAH was induced via filament perforation model. Two photon microscopy was accomplished at different time points after the bleeding, tracking the rhodamine PFCE positive cells *in vivo.* Quantum Dots, CX3Cr1 eGFP mice and rhodamine labelling of PFCEs were used to further elucidate the exact location of the nanoparticles, confirming a colocalization of PFCEs in CX3Cr1 eGFP positive cells. To further investigate the lymphatic clearance of rhodamine PFCE positive cells, we performed immunofluorescence with i.c.m. injection of LYVE-1 and usage of the rhodamine labelling of the PFCEs.
**Results:** Rhodamine labelled PFCEs accumulate in the superior subarachnoid space and the attached leptomeninges after SAH, calculated as summed up intensity levels in defined z-stacks in two photon microscopy. Immunofluorescence staining confirmed colocalization of PFCEs and activated immune cells incl. neutrophil granulocytes and microglia.
**Conclusion:** PFCE nanoparticles may aid in visualizing blood cell clearance and inflammatory cell activation following SAH, representing an imaging tool to study new treatment modalities.

**Resolution of endothelial dysfunction in the course of endotoxemia in young and aged mice measured by MRI in vivo**

Barbara Sitek, Anna Bar, Stefan Chłopicki

Jagiellonian Centre for Experimental Therapeutics (JCET), Jagiellonian University, Kraków, Poland

Sepsis is associated with high mortality especially in the elderly patients, Endothelial dysfunction occurring in sepsis promotes multiple organ failure and mortality but the mechanisms responsible for the resolution of endothelial dysfunction during systemic inflammation such as endotoxemia are not explored.
The aim of this study was therefore to investigate the mechanisms involved in the development of endothelial dysfunction and recovery of normal function in a model of LPS-induced endotoxemia in young and aged mice, with the far-fetched aim to find a pharmacological path to accelerate this process.
The study involved young (3-6 months) and aged (9-12 months) male C57BL/6 mice in which endotoxemia was induced by intraperitoneal administration of a single dose of LPS (3 mg/kg) to assess the endothelial function in vivo by MRI using protocol used in our previous studies (A Bar et al., 2016, NMR in Biomed; A Bar et al., 2019, JAHA; A Bar et al., 2020, JAHA). Vasomotor responses in the thoracic and abdominal aorta were examined by comparing 2 time-resolved 3D images of the vessels before and 25 minutes after intraperitoneal acetylcholine administration. In addition, biochemical analysis in the blood was performed to monitor LPS-induced organ injury.
Results of the experiments indicated that in young mice endothelial function was significantly impaired 12 hours after LPS injection, but then returned to the normal state after 24 hours. However, in aged mice endothelial function was significantly impaired after 12 hours and did not return to the normal state after 24 hours. At the same time, the results of biochemical tests indicated that older mice had significantly greater liver and kidney damage due to endotoxemia than young mice.
In conclusion, our results suggest that an impaired ability of endothelial dysfunction recovery after systemic inflammatory insult by LPS may contribute to the worse course of sepsis and higher organ injury in older mice.

**Multiple sclerosis disrupts natural age-related changes in the brain - a DTI study**

Zofia Schneider[1], Agnieszka Słowik[2], Artur T. Krzyżak[1]

[1]Faculty of Geology, Geophysics, and Environmental Protection,' AGH University of Krakow,

Krakow, Poland; [2]Neurology Clinical Department, University Hospital, Krakow, Poland

**Introduction:** Diffusion tensor imaging (DTI) provides valuable insight into the structure and integrity of brain tissue, so it can be used both to assess age-related changes in the brain and to measure tissue damage caused by diseases such as multiple sclerosis (MS) [1]. Previous research has primarily focused on age-related diffusion parameter changes in white matter (WM) tracts [2], leaving other brain regions less explored. This study aims to investigate the associations between age and DT metrics in a wide range of brain structures among young and middle-aged healthy adults and MS patients.

**Methods:** The study involved 80 healthy individuals (55 females), aged from 21 to 50 years (mean age ± standard deviation: 34.3 ± 8.2) and 80 MS patients (56 females) aged 21 to 48 (35.4 ± 6.7). All participants had brain MRI acquired in the University Hospital in Krakow, Poland using a 3T Siemens Magnetom scanner. The imaging protocol included a $T_1$-weighted MPRAGE sequence and a spin-echo echo-planar imaging (EPI) sequence with 20 directions of diffusion gradients; b factor of 0, 1000 and 2000 s/mm2; TR, 3900 ms; TE, 88 ms; voxel size, 2.5 x 2.5 x 2.5 $mm^3$; field of view, 191 x 191 $mm^2$; number of slices, 50. Each brain was segmented into 95 anatomical structures using the Fast Surfer (FS) software [3]. The DT was calculated using the b-matrices obtained using BSD, a method for reducing systematic errors [4]. The analysis included 21 DTI parameters, comprising fractional anisotropy (FA), axial (AD), radial (RD), and mean diffusivity (MD), DT elements, eigenvalues and invariants, ultimate anisotropy indices and lattice index [5].

**Results:** For the healthy group, we discovered a statistically significant correlation between age and all examined parameters in at least one ROI. The structures most sensitive to age appeared to be the cerebral cortex and its parts, such as the posteriorcingulate, precentral, and postcentral, where the Pearson's correlation coefficient *r* between age and some DT metrics (e.g., MD and AD) exceeded 0.5. Additionally, significant correlations occurred in regions such as the right thalamus, caudate, putamen or cerebellar cortex and WM. For MS patients, most of the correlations apparent for healthy subjects did not occur or were of much lower strength. For example, in the cerebral cortex as a whole for MS patients there were no correlations with any parameter of strength above 0.3. Intriguingly, in certain ROIs (e.g. left supramarginal), healthy subjects showed correlations with diffusivity parameters (e.g. MD or $I_3$), whereas patients with MS showed correlations with anisotropy indices (like FA or UA).

**Conclusion:** Our study showed that certain structures in the healthy brain (mainly composed of GM) undergo age-related changes even in the first half of life. In addition, the same correlations were not apparent for MS patients. Such results may indicate that the impact of disease on the brain structures outweighs the impact of aging, even in normal-appearing tissue. Our results may contribute to better understanding of both neurodegeneration and the influence of MS on central nervous system.

Acknowledgements:
The work was financed by Medical Research Agency contract no: 2020/ABM/01/00006-00.

References:

1. Inglese M. et al. NMR Biomed (2010) 2. Cox S. et al. Nat. Commun. (2016). 3. Henschel L. et al. NeuroImage (2020). 4. Krzyżak A. et al. Magn. Reson. Imag. (2015). 5. Kingsley P. Concepts in Magnetic Resonance Part A (2006).

## Non-invasive determination of oxygen partial pressure in ischemic tissue by $^{19}$F MR relaxometry

Nicolas Stumpe[1], Tuba Güden-Silber[1], Rebekka Schneckmann[2], Katharina Wolters[2], Maria Grandoch[2], Ulrich Flögel[1]

[1]Institute for Molecular Cardiology, Heinrich Heine University, Düsseldorf, Germany; [2]Institute for Translational Pharmacology, Heinrich Heine University, Düsseldorf, Germany

Circulatory disorders and the hypoxia they cause in organs are among the most frequent causes of death in industrialized countries. However, methods for non-invasive

assessment of tissue oxygen level are lacking. The use of physiologically inert perfluorocarbon nanoemulsion (PFC) offers a potential solution for noninvasive determination of tissue partial pressure of oxygen ($pO_2$) using fluorine magnetic resonance imaging ($^{19}$F MRI). The method exploits the property of PFCs that they dissolve oxygen in proportion to the ambient $pO_2$, which leads to a linear change in the $^{19}$F relaxation rate $R_1$[1]. To acquire the $^{19}$F $T_1$ relaxation times a flow sensitive alternating inversion recovery echo planar imaging sequence (FAIR-EPI) at 9.4T was used. A 20% perfluoro-15-crown-5 ether nanoemulsion[2] was used to record the relation between the relaxation rate $R_1 = 1/T_1$ to the surrounding $pO_2$ and the temperature in a three-dimensional surface-plot. $^{19}$F MR relaxometry was applied to determine tissue $pO_2$ in a murine hindlimb ischemia model (HLI)[3]. For this purpose, an occlusion was placed at the femoral artery in the left hind leg. To examine $pO_2$, 100 µl of PFCs were injected bilaterally into the muscles of the upper legs and 50 µl into the lower leg. FAIR-EPI sequence was used to quantify $^{19}$F $T_1$ for the ischemic and control hindlimb one day after surgery. Optimization of the sequence, by rescaling the trajectories of $^{1}$H reference scans, ghosting artefacts for $^{19}$F scans could be eliminated. Through the phantom experiments, a linear relationship was found between $^{19}$F relaxation rate $R_1$ to $pO_2$ and temperature. In the in vivo experiments, the sham hindlimb showed a $pO_2$ of 31.2+7.2 mmHg (n=9). A significant decrease of $pO_2$ to 13.0+6.9 mmHg could be found in the ischemic upper leg. In the experiments of the carves a similar $pO_2$ was found for the sham hindlimb (29.3+10.9 mmHg, n=3), while the $pO_2$ in the ischemic hindlimb decreased even further (6.8+13.9 mmHg, n=3). The values measured in this study are in the same range as the literature values. In conclusion, the non-invasive method of determining partial pressure of oxygen using $^{19}$F MR relaxometry offers a good alternative to the previous highly invasive methods. This has been demonstrated in the example of a murine hind limb ischemia model. Since similar PFCs have already been investigated in clinical studies, clinical translation of the method is highly promising.

References:
1. Chapelin F et al. Prognostic value of fluorine-19 MRI oximetry monitoring in cancer. Mol Imaging Biol. 2022;24(2):208-219.
2. Flögel U et al. In vivo monitoring of inflammation after cardicac and cerebral ischemia by fluorine magnetic resonance imaging. Circulation 2008;118(2):140-148.
3. Schneckmann R et al. Endothelial hyaluronan synthase 3 augments postischemic arteriogenesis through CD44/eNos signaling. Arterioscler Thromb Vasc Biol. 2021;41(10):2551-2562.

**Innovative Liposomal Contrast Agent for Advanced MRI Diagnostics**

Michał Wieteska[1,2], Lucyna Matusewicz[3], Aleksander Czogalla[3], Grzegorz Domański[1], Piotr Bogorodzki[1,2]

[1]Institute of Radioelectronics and Multimedia Technology, Warsaw University of Technology; Warsaw, Poland; [2]Mossakowski Medical Research Institute, Polish Academy of Sciences, Warsaw, Poland; [3]Department of Cytobiochemistry, Faculty of Biotechnology, University of Wroclaw, Wroclaw, Poland

The use of contrast agents in MRI has long been a standard practice to enhance the visibility of specific tissues or anomalies. While conventional gadolinium-based agents have been the cornerstone of this approach, recent developments have introduced other innovative options. Our research delves into the characterization of these novel contrast agents.

We employed the Bruker BioSpec 70/30 USR 7 T MRI scanner to measure the magnetic properties ($T_1$ and $T_2$ relaxation times) of various contrast agents. This included Superparamagnetic Iron Oxide (SPIO) nanoparticles with core diameters of 10, 15, 20, 25, 30 nm (Ocean Nanotech), conventional gadolinium-based contrast agent (Gadovist, Bayer Pharma), as well as an experimental contrast agent consisting of liposomes with DTPA-BSA(Gd) incorporated into liposomal bilayer. We performed our measurements for

various dilutions of these formulations and plotted the calculated relaxation times against the Fe/Gd concentration per milliliter of the sample.

Our findings provide insights into the magnetic properties of each contrast agent. The SPIO nanoparticles, with their diverse sizes have been known to demonstrate remarkable potential for liver imaging and lymph node mapping, offering high contrast and sensitivity [1]. Meanwhile, liposomes with DTPA-BSA(Gd) exhibit great promise, not only as effective contrast agents but also for theranostic applications, highlighting their versatility in cancer diagnostics and therapy [2]. We compare the magnetic properties of the investigated contrast agents and discuss the viability of the experimental liposomal contrast for pre-clinical research.

Acknowledgements.
L.M. and A.C. acknowledge financial support from Polpharma Scientific Foundation, Warsaw, Poland (project no 4/XVI/2017).

References

1. Yì Xiáng J. Wáng, Jean-Marc Idée, A comprehensive literatures update of clinical researches of superparamagnetic resonance iron oxide nanoparticles for magnetic resonance imaging, Quantitative Imaging in Medicine and Surgery 7 (1) (2017), 88-122.

2. C.J. Thébault et al., Theranostic MRI liposomes for magnetic targeting and ultrasound triggered release of the antivascular CA4P, J. Control. Release 10:332 (2020), 137-148.

# Attendees List

**Mitchell Albert**
Lakehead University/Thunder Bay Regional Research Institute
Thunder Bay, Canada

**Francesca Baldelli Bombelli**
Politecnico Di Milano
Milan, Italy

**Anna Bar**
Jagiellonian Centre for Experimental Therapeutics (JCET)
Cracow, Polska

**Ewelina Baran**
University of the National Education Commission
Cracow, Poland

**Silvester Bartsch**
Medical University of Vienna
Vienna, Austria

**Abdel Bidar**
Astrazeneca R&D
Mölndal, Sweden

**Barbara Blasiak**
Institute of Nuclear Physics Polish Academy of Sciences
Cracow, Polska

**Barbara Blicharska**
Marian Smoluchowski Institute of Physics of the Jagiellonian University
Cracow, Poland

**Philipp Boehm-Sturm**
Department of Experimental Neurology, Charité - Universitätsmedizin Berlin
Berlin, Deutschland

**Piotr Bogorodzki**
Warsaw University of Technology
Warsaw, Poland

**Łukasz Boguszewicz**
Maria Sklodowska-Curie National Research Institute of Oncology
Gliwice, Poland

**Susann Boretius**
Leibniz Institute for Primate Research
Göttingen, Germany

**Jeff Bulte**
Johns Hopkins University
Baltimore, Mayland

**Monica Carril**
Instituto Biofisika
Leioa, Spain

**David Červený**
Institute of Clinical and Experimental Medicine
Prague, Czech Republic

**Marian Cholewa**
University of Rzeszów
Rzeszow, Poland

**Karen Cristina Contreras**
Synthetic and Industrial Chemistry at Biofisika Institute
Leioa, Spain

**Piotr Czerwiński**
Comef sp. z o. o. sp. k.
Warsaw, Poland

**Robbin de Kruijf**
Cenya Imaging Bv.
Wageningen, Netherlands

**Monika Drabik**
Mossakowski Medical Research Institute, Polish Academy of Sciences
Warsaw, Poland

**Dominik von Elverfeldt**
Uniklinik Freiburg
Freiburg, Germany

**Cornelius Faber**
University of Münster
Münster, Germany

**Henryk Figiel**
Humanitas University
Sosnowiec, Poland

**Vera Flocke**
University Hospital Düsseldorf
Düsseldorf, Germany

**Ulrich Flögel**
Heinrich Heine University
Düsseldorf, Germany

**Jochen Franke**
Bruker BioSpin
Ettlingen, Deutschland

**Joachim Friske**
Medical University Vienna
Vienna, Austria

**Joanes Grandjean**
Radboud University Medical Center
Nijmegen, The Netherland

**Dominik Havlíček**
Institute for Clinical and Experimental Medicine
Prague, Czechia

**Verena Hoerr**
University Hospital Bonn
Bonn, Germany

**Karolina Janiszewska**
Warsaw University of Technology
Warsaw, Poland

**Krzysztof Jasiński**
Institute of Nuclear Physics Polish Academy of Sciences
Cracow, Poland

**Daniel Jirák**
Institute for Clinical and Experimental Medicine
Prague, Czech Republic

**Natalia Jirát-Ziółkowska**
Institute for Clinical and Experimental Medicine
Prague, Czech Republic

**Radovan Jirik**
Institute of Scientific Instruments, Czech Academy of Sciences
Brno, Czech Republic

**Katarzyna Kalita**
Instuitute of Nuclear Physics Polish Academy of Sciences
Cracow, Poland

**Piotr Kozlowski**
Physics and Astronomy, University of British Columbia
Vancouver, Canada

**Tomasz Krawczyk**
Silesian University of Technology
Gliwice, Poland

**Julia Krystowczyk**
University of Białystok
Białystok, Polska

**Teobald Kupka**
Opole University, Faculty of Chemistry
Opole, Poland

**Grzegorz Kwiatkowski**
Jagiellonian University
Cracow, Poland

**Łukasz Łabieniec**
University of Bialystok
Bialystok, Poland

**Radosław Leszczyński**
RHL-Service
Poznań, Polska

**Yayu Li**
University medical center Freiburg - University of Freiburg
Freiburg, Germany

**Kamil Lipiński**
Politechnika Warszawska
Warsaw, Polska

**Natalia Łopuszyńska**
Institute of Nuclear Physics Polish Academy of Sciences
Cracow, Poland

**David MacDonald**
Institute of Nuclear Physics Polish Academy of Sciences
Cracow, Poland

**Natalina Makieieva**
University of Opole
Opole, Poland

**Alvja Mali**
Wageningen University & Research
Wageningen, Netherlands

**Harald Möller**
Max Planck Institute for Human Cognitive and Brain Sciences
Leipzig, Germany

**Claudia Oerther**
Bruker
Ettlingen, Deutschland

**Zbigniew Olejniczak**
Institute of Nuclear Physics Polish Academy of Sciences
Cracow, Poland

**Martin Pichotka**
University medical center Freiburg - University of Freiburg
Freiburg, Germany

**Sebastian Plona**
Akademia Humanitas
Chorzów, Polska

**Bartosz Pomierny**
Jagiellonian University Medical College
Cracow, Poland

**Pia Pötschner**
Department of Neurosurgery, Charité - Universitätsmedizin Berlin
Berlin, Deutschland

**Wilfried Reichardt**
University medical center Freiburg - University of Freiburg
Emmendingen, Deutschland

**Wojciech Rutkowski**
Institute of Nuclear Physics Polish Academy of Sciences
Cracow, Polska

**Zofia Schneider**
AGH University of Cracow
Cracow, Poland

**Felix Schoknecht**
Department of Neurosurgery, Charité - Universitätsmedizin Berlin
Berlin, Germany

**Barbara Sitek**
Jagiellonian Centre for Experimental Therapeutics (JCET)
Cracow, Poland

**Kamil Stachurski**
Institute of Nuclear Physics Polish Academy of Sciences
Cracow, Poland

**Greg Stanisz**
Sunnybrook Research Institute
Toronto, Canada

**Anna Stefańska**
AGH University of Cracow
Cracow, Poland

**Nicolas Stumpe**
Heinrich Heine University
Düsseldorf, Germany

**Peter Vermathen**
MR Methods, DIN & DBMR, University & Inselspital
Bern, Switzerland

**Jens Waldeck**
Bruker BioSpin GmbH & Co KG
Ettlingen, Germany

**Władysław Węglarz**
Institute of Nuclear Physics Polish Academy of Sciences
Cracow, Poland

**Marlena Wełniak-Kamińska**
Mossakowski Medical Research Institute, Polish Academy of Sciences
Warsaw, Poland

**Astrid Wietelmann**
Max-Planck-Institute for Heart and Lung Research
Bad Nauheim, Germany

**Michał Wieteska**
Warsaw University of Technology
Warsaw, Poland

**Anton Windfelder**
Fraunhofer IME Department
Bioresources
Giessen, Germany

**Juan Yang**
SINTEF
Oslo, Norway

**Igor Zhukov**
Institute of Biochemistry and Biophysics
Polish Academy of Sciences
Warsaw, Poland

# Maps

Adresses:

**The H.Niewodniczański Institute of Nuclear Physics PAS**

Radzikowskiego 152; 31-342 Krakow

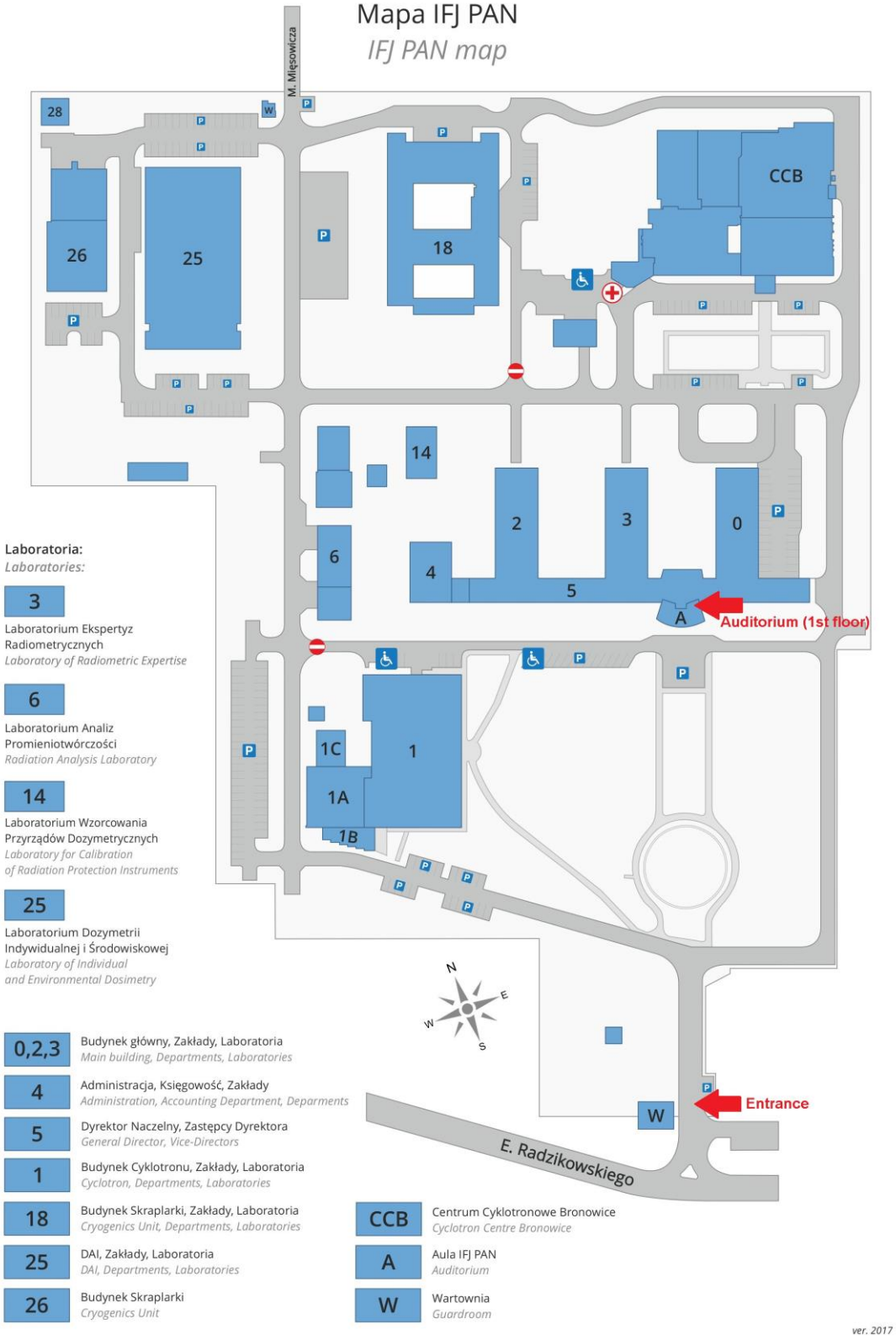

**Cracow public transport homepage (english):**
[KMK Public transport – ZTP Kraków]

**Cracow public transport network map:**
[KMK maps – ZTP Kraków]